(51) International Patent Classification 6 : G02B 21/24, 21/26, 7/36	A1	(11) International Publication Number: WO 96/01438
		(43) International Publication Date: 18 January 1996 (18.01.96)

(21) International Application Number: PCT/US95/08424

(22) International Filing Date: 30 June 1995 (30.06.95)

(30) Priority Data:
08/270,017   1 July 1994 (01.07.94)   US

(60) Parent Application or Grant
(63) Related by Continuation
US   08/270,017 (CIP)
Filed on   1 July 1994 (01.07.94)

(71)(72) Applicant and Inventor: PRICE, Jeffrey, H. [US/US]; 8568 Villa La Jolla Drive #290, La Jolla, CA 92037 (US).

(74) Agents: BAKER, Freling, E. et al.; Baker, Maxham, Jester & Meador, Suite 2770, 750 B Street, San Diego, CA 92101 (US).

(81) Designated States: AM, AT, AU, BB, BG, BR, BY, CA, CH, CN, CZ, DE, DK, EE, ES, FI, GB, GE, HU, IS, JP, KE, KG, KP, KR, KZ, LK, LR, LT, LU, LV, MD, MG, MN, MW, MX, NO, NZ, PL, PT, RO, RU, SD, SE, SG, SI, SK, TJ, TM, TT, UA, UG, US, UZ, VN, European patent (AT, BE, CH, DE, DK, ES, FR, GB, GR, IE, IT, LU, MC, NL, PT, SE), OAPI patent (BF, BJ, CF, CG, CI, CM, GA, GN, ML, MR, NE, SN, TD, TG), ARIPO patent (KE, MW, SD, SZ, UG).

Published
With international search report.

(54) Title: AUTOFOCUS SYSTEM FOR SCANNING MICROSCOPY
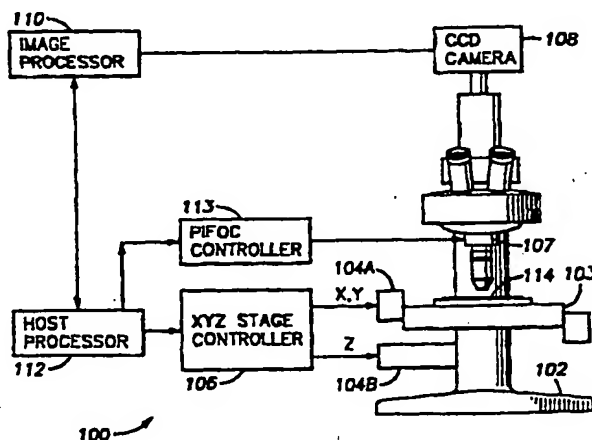
(57) Abstract

Reliable autofocus is required to obtain accurate measurements of fluorescent stained cellular components from a system capable of scanning multiple microscope fields. Autofocus could be performed directly with fluorescence images, but due to photobleaching and destructive fluorescence by-products, it is best to minimize fluorescence exposure for photosensitive specimens and live cells. This exposure problem could be completely avoided by using phase-contrast microscopy, implemented through the same optics as fluorescence microscopy. Functions for both phase-contrast and fluorescence autofocus were evaluated using the present invention and the suitability of phase-contrast autofocus for fluorescence microscopy was determined. The present autofocus system for scanning microscopy can be performed at least as fast as 0.25 s/field without loss of precision. The speed of autofocus can be further increased by a volume image which is obtained by observing an image object at each image plane of a plurality of image planes, where each image plane is vertically displaced with respect to each other image plane. An electronic image representation is obtained at each image plane. The image planes are scanned over the image object and the images are aligned timewise in a buffer. The buffer holds a volume image comprising images at the image planes, aligned by the buffer. The image plane having the best focus is selected and a microscope objective is automatically positioned at the selected plane.

1

DESCRIPTION

AUTOFOCUS SYSTEM FOR SCANNING MICROSCOPY

MICROFICHE APPENDIX

A Microfiche Appendix containing computer source code is attached. The

5 Microfiche Appendix comprises one (1) sheet of microfiche having 22 frames, including one title frame.

The Microfiche Appendix contains material which is subject to copyright protection. The copyright owner has no objection to the reproduction of such material, as it appears in the files of the Patent and Trademark Office, but

10 otherwise reserves all copyright rights whatsoever.

TECHNICAL FIELD

The present invention relates to autofocusing and, more particularly, to a system for microscope autofocusing.

BACKGROUND ART

15 Autofocus is a requirement for any fully automated microscope-based image processing system that must scan areas larger than a single field. Experience has shown that it is not possible to maintain focus simply by determining the best foci at two points on a microscope slide and scanning along the line between them in three dimensional space. This may be due to many

20 causes, including mechanical instability of the microscope and irregularity of glass slide surfaces. For example, thermal expansion could account for several microns of instability in microscopes with lamps acting as unevenly distributed heat sources. Using the coefficient of thermal expansion for aluminum, a $1.0^{\circ}C$ increase causes 0.6 micrometer (μm) of expansion for each 25 millimeters (mm)

25 length between the objective and stage in a microscope. Mechanical instability

may also arise from gear slippage and settling between moving components in the stage. Microscope slide surface irregularity is another source of error. Standard optical quality mirror flatness is about 1.5 μm over 25 mm. Given that mirrors are ground glass and microscope slides are float glass, microscope slide surface

5 irregularity could be much greater. According to the definition by others, such as Françon (Françon M: Progress in Microscopy. Row, Peterson, Evanston, Ill., 1961), the theoretical microscope depth of field for an objective with numerical aperture (NA) 0.75 is 0.74 μm at a wavelength of 500 nm. Best focus can vary through a range of about 25 μm in a horizontal scan of 50 mm across a

10 microscope slide. Whatever the source of instability, autofocus can compensate given that the positional variations have relatively long time constants.

Most autofocus methods fall into two categories: position sensing and image content analysis. Position sensing methods, such as interferometry, require independent calibration of the best focus location and, more importantly, a single

15 well-defined surface from which to reflect light or sound. In light microscopy there are often two reflective surfaces, the coverslip and slide. In addition, tissue specimens can have significant depth and best focus is not necessarily achieved at the surface of the glass. These problems make absolute position sensing methods impractical for use in light microscopy. Image content analysis functions, such as

20 used by the present invention for autofocusing the microscope, on the other hand, depend only on characteristics measured directly from the image. Best focus is found by comparison of these characteristics in a series of images acquired at different vertical positions. This method of autofocus requires no independent reference and is not affected significantly by the second reflective surface. Its

25 most important limitation is speed, which is dependent on the video rate, the vertical repositioning time, function calculation time and search range.

Image content autofocus functions have previously been compared for brightfield microscopy, but apparently not for fluorescence or phase-contrast

3

microscopy. For example, Groen, Young and Ligthart (Groen FCA, Young IT, Ligthart G: A comparison of different focus functions for use in autofocus algorithms. Cytometry 6:81-91, 1985) compared 11 autofocus functions under brightfield using an electron microscope grid and a metaphase spread, and Vollath

5   (Vollath D: Automatic Focusing by Correlative Methods. J Microsc 147:279-288, 1987) tested an autocorrelation function under brightfield using a pearlitic steel specimen. Groen et al. concluded that three autofocus functions, i.e., two gradient functions and the intensity variance, performed the best. However, some autofocus functions that performed well on one specimen did not perform well on others and

10   the authors cautioned against extrapolating the results to other imaging modes and specimens.

The uncertainty in applying autofocus test results from one microscope method to another led to the present invention. The development of the present invention included exploring autofocus performance in microscopy of fluorescent

15   stained biologic specimens. The fluorescent signal can be used directly for autofocus. However, problems summarized by others, such as Chen (Chen LB: Fluorescent labeling of mitochondria, in Fluorescence Microscopy of Living Cells in Culture, Part A, Wang YL and Taylor DL, eds. Academic Press, San Diego, 103-123, 1989), including photobleaching and the formation of free radicals,

20   singlet oxygen, and heat, can create conditions under which minimizing fluorescent excitation becomes critical. The most critical conditions probably occur in analyzing live cells. If the signal is weak and antiphotobleaching agents cannot be used because of toxicity, the signal could easily be completely lost in the 5 - 10 video frames of exposure required for autofocus. In addition, the fluorescence

25   byproducts themselves are toxic, and excessive exposure could alter the results or damage living cells. Therefore it is desirable to find a nondestructive imaging technique for autofocus. With brightfield microscopy, fluorescent stained cells appear unstained, showing very little contrast. Phase-contrast microscopy, on the

4

other hand, gives high contrast images of unstained cells and is more useful for autofocus. For these reasons, autofocus function performance was tested for both phase contrast and fluorescence microscopy. More details of different approaches for autofocus can be found in the doctoral dissertation of Jeffrey H. Price entitled

5   Scanning Cytometry for Cell Monolayers, University of California, San Diego, 1990, which is hereby incorporated by reference.

DISCLOSURE OF INVENTION

The present solution to the problem of fast and reliable autofocus of cellular components from photosensitive specimens and live cells in a system

10   capable of scanning multiple microscope fields is the instant autofocus system for scanning microscopy designed to automate, simplify, accelerate, and improve the quality of the process. The goal of the autofocus system is to accurately and automatically position the focus positioner, or focus mechanism, of the microscope so as to gather information and present it for further processing.

15   BRIEF DESCRIPTION OF DRAWING

The objects, advantages and features of this invention will be more readily appreciated from the following detailed description, when read in conjunction with the accompanying drawing, in which:

Fig. 1 is a high-level diagram illustrating the basic components of a

20   presently preferred embodiment of the autofocus system of the present invention;

Figure 2 is a representation of a magnified image of cells as seen through the microscope of the system shown in Figure 1;

Figure 3 is a block diagram of the presently preferred image processor of Figure 1;

25   Figure 4 is a high-level flow diagram of an autofocus process performed by the system shown in Figure 1;

5

Figure 5 is a flow diagram of a binary search autofocus process performed by the system shown in Figure 1;

Figure 6 is a flow diagram of a sequential autofocus process performed by the system shown in Figure 1;

5   Figures 7a, 7b, 7c, 7d, 7e, 7f, 7g, 7h, and 7i illustrate autofocus function (F_1-F_{11}) results for a microscope field containing 10 fluorescent stained cells using the system shown in Figure 1;

Figures 8a, 8b, 8c, 8d, 8e, 8f, 8g, 8h, and 8i illustrate autofocus function (F_1-F_{11}) results for a phase contrast microscope field containing 10 cells using the

10   system shown in Figure 1;

Figures 9a, 9b, 9c, 9d, 9e, 9f, 9g, 9h, and 9i illustrate autofocus function (F_1-F_{11}) results for a microscope field containing a single fluorescent stained cell using the system shown in Figure 1;

Figures 10a, 10b, 10c, 10d, 10e, 10f, 10g, 10h, and 10i illustrate autofocus

15   function (F_1-F_{11}) results for a phase contrast microscope field containing a single cell using the system shown in Figure 1;

Figure 11 is a three-dimensional plot of the response of function F_3 against focus position and zoom using the system shown in Figure 1; and

Figure 12 is a chart showing experimental results in autofocus precision,

20   accuracy and speed for the phase contrast and fluorescence methods.

Figure 13 is a microscopic system schematic that illustrates the operation of an autofocus system using volume imaging according to the invention;

Figures 14A and 14B are block diagrams of a first embodiment of a volume imaging apparatus;

25   Figures 15A and 15B are diagrams of a second embodiment of a volume imaging apparatus;

Figure 16 illustrates a microscope field being scanned by a volume imaging array according to the invention;

6

Figure 17 is an illustration of a buffer for image alignment in the volume imaging apparatus;

Figure 18 is a schematic representation of a volume image stored in a buffer of Figure 17;

5   Figure 19 is a flow diagram illustrating the autofocus procedure using the volume imaging apparatus;

Figure 20 is a plot showing a optical quality metric for best focus selection using volume imaging; and

Figure 21 is an embodiment of a volume imaging autofocus system using
10   optical highpass filtration.

BEST MODES FOR CARRYING OUT THE INVENTION

AUTOFOCUS BY VERTICAL POSITIONING

The following detailed description of preferred embodiments of autofocusing by vertical repositioning presents a description of certain specific
15   embodiments to assist in understanding the claims. However, the present invention can be embodied in a multitude of different ways as defined and covered by the claims.

For convenience, the following description is topicalized into the following principal sections: I. *Materials and Methods*, II. *Metrics for Performance:*
20   *Autofocus Functions*, III. *Performance Results*, and IV. *Conclusions*. A more detailed outline of the description is as follows:

I.   MATERIALS AND METHODS
        A.   Microscope and Image Processor Overview
        B.   Microscope and Video Camera
25   C.   Positioners

7

I. MATERIALS AND METHODS

A. Microscope and Image Processor Overview

Figure 1 illustrates the presently preferred embodiment of an autofocus system 100 of the present invention which uses vertical positioning to acquire

8

focus information. The hardware components of the system 100 include an epifluorescent microscope 102, a motorized stage 103, controlled by a pair of XY motors 104a and a Z motor 104b, XYZ stage controller 106, a piezoelectric positioner 107, a video camera 108, an image processor 110, and a host processor 5 112. These components are further described below.

B. Microscope and Video Camera

In one presently preferred embodiment, the cells (Figure 2) are imaged on a Nikon Optiphot 102 (Figure 1) through a CF Fluor DL 20x C, 0.75 NA objective with Ph3 phase contrast. This fluorite objective provides high UV 10 transmission. The epifluorescence filter cube has a 365 nm ± 10 nm (50% of peak) bandpass excitation filter, a 400 nm dichroic mirror and no barrier filter. In experiments, the images were further magnified through a Nikon CCTV 0.9 - 2.25 zoom lens onto a Dage VE 1000 RS-170 CCD camera 108. Experiments were performed at a zoom of 1.0 except for the sampling experiments, which were 15 carried out at a series of magnifications. For phase contrast, a Nikon 0.52 NA long working distance condenser is used.

C. Positioners

The microscope stage 103 (Figure 1) is moved laterally under computer control by stepper motors. The stage 103 is built by Syn-Optics (Sunnyvale, CA) 20 and modified by New England Affiliated Technologies (Lawrence, MA) for finer stepping and simpler computer control. The smallest step size is 0.127 μm. The stage 103 is controlled by a New England Affiliated Technologies 103M microstepping driver and an Oregon Micro Systems, Inc. (Beaverton, OR) PCX AT ISA-bus compatible computer board.

25 Focus is changed with a piezoelectric objective positioner ("PIFOC") 107 and an E-810.10 closed loop controller (Polytech PI, Costa Mesa, CA). The piezo

9

positioner 107 is sandwiched between the objective turret and the objective of the microscope 102. Measurements with an oscilloscope reading the built-in linear variable differential transformer (LVDT) sensor output showed that movements of < 1 μm occurred in < 10 milliseconds (ms) with the fluorite objective, and

5   response was dependent on objective mass. To retain the 160 mm tube length of the Optiphot 102, the objective turret is replaced by a custom-machined adapter. The 13 mm thick objective positioner significantly reduces image quality if this is not done, but movement through the 100 μm (0.004") range does not measurably degrade the image. Position is controlled by output from a digital-to-

10   analog converter in a Keithley Metrabyte (Taunton, MA) DAS-1600 Data Acquisition Board. The 12-bit D/A converter divides the 100 μm range of the PIFOC 107 into 4096 steps of 24 nm each. Due to the previously discussed temperature and mechanical instabilities of the microscope 102 itself, actual focus accuracy is not better than a few microns over long periods, but for the required

15   focus interval of a fraction of a second, the precision approaches the minimum step size.

D. Lamps and Exposure Control

     For fluorescent autofocus tests, specimen exposure is controlled with a Uniblitz Model D122 Driver and Shutter (Vincent Associates, Rochester, NY).

20   The fluorescence lamp is an Osram 100w HBO W/2 mercury vapor arc lamp in a Nikon HMX-2 lamp house. Variability of < ±3% over 3 hours with this lamp is measured by illumination of the cell stain solution described above, modified by an addition of 10 μg/ml DAPI and 1 mg/ml Herring Sperm DNA (Sigma, St. Louis). This solution is placed in an acrylic well under a sealed coverslip. For

25   phase contrast, exposure is controlled with an EG&G Electro-Optics PS 450AC Power Supply (Salem, MA) and an XSA 80-35S-30171 xenon flash lamp (Advanced Radiation Corp., Santa Clara, CA). A Nikon HMX-2 lamp house was

modified to house the xenon flash lamp and wired to the 450AC power supply. The strobe is triggered by the timer circuit on the data acquisition board. The timing for the strobe is supplied by a vertical blank hardware interrupt from the image processor 110 (Figure 1). The data acquisition board has a programmable

5   strobe delay that is set for 14 ms to assure that the objective positioner has completed movement prior to image acquisition. The strobe rate is 60 Hertz (Hz) during phase contrast focus testing. The average stability of this lamp is better than the mercury vapor arc lamp, but there are occasional intensity spikes.

To perform an autofocus calculation in real time, either the focus position
10   has to be moved in less than 16 ms (for 60 Hz operation), or the position has to be moved at a constant velocity and the image frozen with a strobe. For the best performance with the incremental movement utilized herein, the image is collected after movement has been completed. This is done in phase contrast by delaying the strobe 14 ms after the vertical blank in the video signal (when the command

15   to change position is sent to the PIFOC 107). This delay insures that the focus position has changed before the image is collected by the video camera 108. The 14 ms delay and the strobe would not be required if the position could be changed during the vertical blank interval of about one ms. Better feedback control electronics on the PIFOC 107 would allow movement to occur fast enough to

20   eliminate the need for the strobe.

E. Image Processor, Computer and Software

An Imaging Technology, Inc. Series 151 Image Processor 110 (Figure 1) is used for speeding image operations. A block diagram of the preferred image processor 110 is illustrated in Figure 3. It should be observed that while an image

25   processor 110 will generally speed up the autofocus operation of the present invention, if speed is not critical there is no reason why the calculations performed therein could not take place in the host processor 112 (Figure 1) or any other

11

computer. The image processor 110 is preferably configured with six functional
units, or boards, as follows: 1) a 512 x 512 8-bit Variable Scan Interface 130 for
analog to digital conversion of the video signal generated by the camera 108, 2)
a 512 x 512 x 32-bit Frame Buffer 132 for storage of four digital images, 3) a
5   1024 x 1024 x 32-bit Frame Buffer (not shown, but similar connections are made
to the buses of the processor 110 as shown for the frame buffer 132) for storage
of sixteen digital images, 4) a Histogram/Feature Extractor 134 for creating a 10-
bit intensity histogram, 5) a Real Time Modular Processor (RTMP) 138 with a
Real Time Sobel module for 8 x 8 convolutions and a 16-bit look-up-table, and
10   6) an Arithmetic/Logic Unit 136 for multiplication, subtraction, addition and
scaling. The RTMP 138 is a single board with three plug-in connections for sub-
modules. The Real Time Sobel module utilizes two of these connections and the
look-up-table utilizes the third connection. All of these operations proceed at
video rates and can be pipelined for parallel operation.

15   The key components of this system for testing the autofocus functions are
the 8 x 8 convolver (part of RTMP 138) and the histogrammer 134. For most of
the autofocus functions, the image is convolved and then histogrammed in a single
pipelined video frame or field. The histogram is used to calculate the intensity
sum, sum of squares and statistics, e.g., variance or standard deviation, with
20   filtered image results truncated to 8 or 10 bits/pixel. The calculation results are
further used to calculate a measure of focus. For 16-bit calculations, the image is
first transferred to the host computer. Small differences are sometimes observed
between the 8-bit and 10-bit results, but no further improvement is observed
utilizing 16-bit results. Therefore, only 10-bit data for autofocus of selected fields
25   is reported. For the presently preferred 60-Hz scanning implementation, the
absolute value of the filtered images is taken prior to truncation to 8 bits. The
host computer 112 (Figure 1) is preferably an AT-compatible 33 megaHertz (MHz)
Intel i486 personal computer (PC).

12

The software programs to implement the autofocus process (Figure 4) and related control functions are written in 'C' and assembler. A portion of the 'C' and assembler source code is included in the attached Microfiche Appendix. The C routines are compiled with Metaware High C (Santa Cruz, CA). A Phar Lap

5   (Cambridge, MA) assembler is used for the interrupt service routines that are running in the background. All object code is linked with the Phar Lap 386 DOS Extender. The Imaging Technology Series 151 C Library source code is also ported to ANSI C and recompiled with Metaware High C. This combination allows use of the full 32-bit capability of the i486 CPU by programs running under

10   16-bit DOS.

F. Cells and Specimen Preparation

A portion of an example specimen, such as the specimen 114 of Figure 1, is shown in Figure 2. Figure 2 represents a magnified image of a typical specimen comprising a set of cells, particularly cell nuclei, generally indicated at 116.

15   In one experiment, NIH 3T3 cells were plated on washed, autoclaved #1.5 coverslips. The cells were maintained in Eagle's minimal essential medium with Earle's salts, supplemented with 10% fetal bovine serum, 100 μg/ml gentamicin, and 0.26 mg/ml L-glutamine (final concentrations), in a humidified 5% CO_2 incubator at 37°C. After 1 day of cell growth, the coverslips were washed in

20   phosphate buffered saline (PBS), fixed for 10 minutes in 4% paraformaldehyde in 60% PBS, and stained for one hour. The stain solution consisted of 50 ng/ml 4',6-diamidino-2-phenylindole dihydrochloride (DAPI, Molecular Probes, Eugene, OR), 10 mM TRIS, 10 mM EDTA, 100 mM NaCl, and 2% 2-mercaptoethanol as described by others, such as Hamada and Fujita (Hamada S, Fujita S: DAPI

25   Staining Improved for Quantitative Cytofluorometry. Histochem 79:219-226, 1983). After staining, a few drops of DAPI solution were placed on a glass slide, the coverslips were laid face down over the solution, excess solution was wicked

13

away with tissue, and the coverslips were sealed to the slide with nail polish. This stain solution was found to exhibit excellent antiphotobleaching properties. Although photobleaching was avoided with this preparation, the degree of photobleaching can vary markedly with different techniques. This specimen also

5   did not exhibit significant autofluorescence, which if nonspecific and diffuse could degrade performance by reducing contrast.

G. Basis for Comparison of Autofocus Functions

There is no independent standard against which autofocus functions can be tested. Therefore, performance must be rated by comparison. Groen et al., loc.

10 . cit., suggests eight criteria for comparing the performance of autofocus functions. These are: 1) unimodality, or the existence of a single maximum or minimum; 2) accuracy, or coincidence of the extremum and best focus; 3) reproducibility, or a sharp extremum; 4) range, or the vertical distance over which the function will unambiguously determine the direction to best focus; 5) general applicability, or

15   the ability to work on different classes of images; 6) insensitivity to other parameters, or independence from influences such as changes in mean intensity; 7) video signal compatibility, or the ability to use the same video signal as is utilized for image analysis; and 8) implementation, that is, it should be possible to calculate the function rapidly.

20   The first three criteria – unimodality, accuracy and reproducibility – are most important for automated scanning. The range is less important because focus is usually performed on a field immediately adjacent to one where best focus was just calculated. Comparisons of microscope autofocus functions performed by Groen et al., loc. cit., led to the conclusion that the fifth criterion, general

25   applicability for all types of images, cannot necessarily be expected. For a scanning system, however, it is sufficient to require applicability to one microscope imaging method (e.g., phase contrast or fluorescence) for all microscope fields.

14

The seventh criterion, video signal compatibility, is hardware dependent and is easily satisfied. The eighth criterion, implementation, is dependent on computer speed and function complexity.

H. General Autofocus Process

5   Referring to Figure 4, a high-level description of the autofocus process 200 will now be given. Note that autofocus is controlled from the host processor 112 (Figure 1). The host processor 112, or the image processor 110 under control of the host processor, can perform a transformation on the image and obtain a value which represents a degree of focus. This value can then be compared with another

10   value obtained from another image after the stage 103 is moved up or down via the XYZ stage controller 106 to indicate the next direction of stage movement or after the objective is adjusted by the PIFOC 107.

        Beginning at a start state 202, the system 100 proceeds to a state 204 to acquire a digital image of the specimen 114 on the stage 103 at a first vertical

15   position. The image is captured by the image processor 110. Moving to state 206, the system 100 applies a filter to the digital image to produce an intermediate or filtered image. The presently preferred embodiment utilizes a digital filter, and more specifically, the image sharpening transformation defined in function F_7 of Table 1. Of course, other filters, including analog filters can be used. Proceeding

20   to state 208, the system 100 applies a measurement function to the intermediate image to obtain a magnitude. The presently preferred embodiment uses a contrast measurement function which utilizes the variance or standard deviation of image intensity, or the sum of the squares of the image intensity. Moving to a decision state 210, the system 100 determines if the Nth image has been acquired. The

25   value of N utilized varies according to the specific autofocus method employed. For the purposes of this discussion, and as an example, N will be equal to two. Therefore, during the first pass of states 204 to 210, only the first image is

15

acquired, and the flow continues at state 212 wherein the stage 103 is moved by Z motor 104b in a vertical direction to a new (second) vertical position. In the preferred embodiment there are two focus mechanisms, therefore the piezoelectric PIFOC positioner 107 is moved instead of the stage 103 for fast autofocus, and

5   both the PIFOC 107 and the stage 103 are to be moved together to combine fast autofocus and extended focus range.

After the stage 103 has been moved to the new vertical position, or the PIFOC 107 adjusts the objective, the flow continues at state 204, wherein a digital image is acquired at the second vertical position. The states 206 and 208 are

10   executed again using the second image to obtain a second magnitude. Moving to state 210, when the Nth image has been acquired, as for the current example of N=2, the system 100 proceeds to state 214. At state 214, the acquired magnitudes are compared and the focus is adjusted based on the results of the comparison. For the current example, if the magnitude at the first vertical position is greater

15   than the magnitude at the second vertical position the focus mechanism is moved toward the first vertical position, else if the magnitude at the first position is less than the magnitude at the second position, the focus mechanism is moved toward the second vertical position. The PIFOC 107 and the vertical stage stepper motor positioner are both focus positioners. The PIFOC is much faster, but has a shorter

20   range (100 μm or 0.004" in the presently preferred model, 200 μm in an alternate embodiment. The stepper motor, moving the entire mass of the stage, rather than just the objective, takes longer and cannot be use din a real time calculation, but has a range limited only by the room between the specimen and objective and the physical design of the microscope. Either or both can be used for autofocus. For

25   a slow system with focus in a few seconds, the stage is fast enough. For a fast system requiring focus in a fraction of a second, the PIFOC 107 is necessary. For applications requiring greater range and fast focus, the stage could be focused first and all subsequent focusing done by the PIFOC 107 until the range is exceeded.

16

The stage could then be adjusted as necessary to keep the PIFOC 107 within its range. After the focus has been adjusted at state 214, the autofocus process 200 completes at an end state 216.

A number of different autofocus functions, which are further discussed
5   below, may carry out one or both of states 206 and/or 208.

The following two section will describe two specific methods utilized for autofocus: binary search and sequential autofocus.

I. Binary Search Autofocus Process

Referring to Figure 5, the binary search autofocus process 250 will now be
10 described. This process is a more specific version of the process 200 shown in Figure 4. Autofocus process 250 uses the well-known binary search algorithm to move the stage 103 (Figure 1) and locate best focus. The search range is fixed as the distance of focus search interval and the center of the range is the center of focus search interval. Binary search autofocus is carried out by defining two focus
15 positions between which focus is thought to exist and sequentially dividing the range in half to narrow down on best focus. The range is narrowed in this manner until it is smaller than the precision needed to identify best focus.

The binary search autofocus process 250 begins at a start state 252, wherein a user, or an automated scanning program, requests focusing. The range is set to
20 an initial value, e.g., 4 microns. The system 100 then moves to a state 254 wherein the focus mechanism is positioned at the center of the focus test range. The focus mechanism is the PIFOC 107 or the stage 103 (note the vertical control is 104b which moves the stage 103 through a series of gears inside the microscope), or both. An image is then acquired, filtered, and histogrammed by
25 using the image processor 110. From the histogram, a single focus function result (Fc) is calculated for that position and stored. Moving to state 256, the focus mechanism is positioned at the beginning of the range, and another image is

17

acquired, filtered, and histogrammed.   Another focus function result (Fa) is calculated and stored as before. Proceeding to state 258, the focus mechanism is positioned at the end of the range, and another image is acquired, filtered, and histogrammed.   From the histogram, a single focus function result (Fb) is

5   calculated for that position and stored as before. States 252 through 258 comprise an initialization sequence of the process.   The rest of the flow chart states represents the loop that is executed to narrow the range until focus is found.

Continuing at a decision state 260, a check (is range less than minimum) is made to see if the desired precision has been achieved. The minimum is user

10   and application dependent. A practical example of the minimum is between 0.001 μm and 1.0 μm depending on the demands of the application. The minimum step size of the presently preferred PIFOC 107 is 0.024 μm and is determined by the digital/analog converter control board in the host computer 112 and the electronics of the PIFOC controller. If the range is small enough focus has been located, and

15   the flow completes at an end state 272. If the range is not less than minimum, as determined at decision state 260, the system 100 continues at state 262 wherein the range is decreased by half. Proceeding to a decision state 264, a determination is made if the focus value result Fa is greater than the result Fb. If Fa, the focus value at the beginning of the range, is greater than Fb, the focus value at the end

20   of the range; then the focus is closer to the beginning of the range. The new range will be defined by the old beginning and the center. If not, the focus is closer to the end of the range and the new range will be defined by the old center and end.

If Fa is greater than Fb, the system moves to state 266, due to the focus value being closer to the beginning of the old range. The system 100 sets the new

25   center to a position between the center and start of the old range, and moves the focus mechanism to the new center. The system also places the focus value (Fc) at the old center into the storage represented by Fb because this is the new end of the range. The system 100 further acquires, filters, histograms and calculates the

18

focus function value for the new image and stores the result in Fc. At the completion of state 266, the system 100 loops back to decision state 260 to determine if the range is now less than minimum, as previously described.

If Fa is not greater than Fb, as determined at decision state 264 and
5   asserted at state 268, the system moves to state 270, due to the focus value being closer to the end of the old range. At state 270, the system 100 sets the new center to a position between the old center and old end of the range, and moves the focus mechanism to the new center. The system also places the focus value at the old center (Fc) into the storage represented by Fa because this is the new start
10   of the range. The system 100 further acquires, filters, histograms and calculates the focus function value for the new image and stores the result in Fc. At the completion of state 270, the system 100 loops back to decision state 260, as previously described.

J. Sequential Autofocus Process

15   Referring to Figure 6, the sequential autofocus process 300 will now be described. The sequential autofocus process 300, which is a more specific version of the autofocus process 200 (Figure 4), begins at a start state 302, wherein a user, or an automated scanning program, requests focusing. The range is set to an initial value, e.g., 4 microns. The system 100 then moves to a state 304 wherein the start
20   position is set to the initial value at the beginning of the range and the position number, n, is set to 0. Moving to state 306, the system 100 begins a loop (states 306 through 310) that positions the focus mechanism and calculates the focus function at each position. The focus mechanism is positioned to the 'start position plus (n times the step size)'. The step size is the same as the "focus increment"
25   in the experimental table of Figure 12. Focus increments of 0.102, 0.195, 0.244, 0.146, 0.220 and 0.073 micrometers were used in those experiments. Then the image is acquired, filtered, histogrammed and the focus function calculated. The

19

result is stored for later calculation of best focus. Proceeding to a decision state 308, the system 100 determines if 'the current position minus the start position $\leq$ range', i.e., whether the focus position sequence finished. If so, the system moves to state 312 to calculate best focus. If not, the system 100 moves to state 310 to

5   increment the position number, n, by one, and continue moving and calculating the focus function results by looping back to state 306.

If the focus position sequence is finished, as determined at decision state 308, the system 100 moves to state 312 and computes the best focus. The power weighted average equation (Equation 1) is used to compute the best focus from the

10   focus function values at positions 0 to z $F_0...F_z$. At the completion of computing the best focus, the system advances to a decision state 314 to determine if the result lies too close to the beginning or end of the range. One example of too close is within 1/4 of the range. If the focus search range is 4 micrometers, and if the focus result were within 1 micrometer of either end of the range, then the

15   center of the range would be repositioned and focus repeated. The actual value may vary depending on the application (specimen, required speed, etc.). If so, the true focus may lie outside the range. The system 100 proceeds to state 316 to change the center to the end of the range closest to calculated focus and repeat the focus sequence by looping back to state 304, as previously described. Note that

20   the range stays the same, but the process succeeds as long as the focus values increase toward best focus. The range can be broadened automatically to speed finding best focus. This feature is important in an application where the focus at an adjacent field is not known, such as for a commercial microscope focus attachment that focuses regardless of the start position. Best focus is achieved if

25   the result is close to the center, as determined at decision state 314, and therefore the system 100 proceeds to state 318 wherein the focus mechanism is positioned at best focus. The sequential autofocus process 300 completes at an end state 320.

20

K. Automated Scanning and Real-Time Focus Calculation

One series of tests on the system 100 involved scanning areas of > 1000 microscope fields in a raster pattern automatically. At each new field the best focus for the previous field is used for the center of the test focus range. The

5   microscope is refocused at the beginning of the test sequence on each field until the calculated best focus fell into the inner half of the test range. This allows best focus to be achieved even if the best focus is outside the initial test range. In practice, the test range was wide enough to make refocusing rare. Before autofocus, the intensity of the fluorescence image is summed to verify the presence

10   of at least one cell. If no cells are present, the field is skipped. At the beginning of a new row, the best focus from the beginning of the previous row is the center of the test range. Before the start of each experiment, a specimen is placed on the microscope, the scanning rectangle chosen, and the corners of the rectangle checked to verify that the foci are within the 100 μm range. At the first field,

15   focus is performed manually. After the first field there is no human intervention until the scan is complete.

Focus is calculated 20 times for both phase contrast and fluorescence on each field for statistical analysis of repeatability and comparison of accuracy. Precision is evaluated by the combined standard deviation of all focus trials from

20   the entire scan. The combined standard deviation is computed by taking the square root of the average variance. Each focus test sequence is performed at 60 Hz by interrupt service routine control. An interrupt is initiated at the beginning of each vertical blank (60 Hz) by the Variable Scan Interface board on the Series 151 Image Processor. The interrupt service routine controls the strobe, and accounts

25   for the 2 vertical blank delay between image integration on the CCD chip (objective positioner movement) and histogram acquisition on the image processor. Accounting for the delay between positioning and image stabilization enables repositioning and measurement to occur at video rates. The path through the

21

image processor is from the digitized image in the Variable Scan Interface through the convolver to the histogrammer. The histogrammer input contains a 2-bank, 10-bit look-up table that is used to separate the odd and even fields for 60 Hz positioning and function calculation. Histogrammer look-up-table bank 0 is

5   programmed to pass the even field unchanged and bank 1 is programmed to add 256 to the odd field. The interrupt service routine switches banks on alternate vertical blanks. At the end of each odd field the interrupt service routine transfers the resulting 9-bit histogram and independently calculates the odd and even sum, sum of squares and pixel count. These values are placed in arrays accessible to

10   'C' routines for final calculation of the best focus position. The function results are also normalized by the number of pixels.

       After each focus sequence, with evaluation of the function at a number of positions, the maximum and the weighted average are used to find best focus. If the cells had been thinner than the depth of field of the microscope and the

15   discrimination range of the focus function, the maximum would have been expected to perform well. In practice, however, the cells are thicker than the depth of field and much thicker than the discrimination range of the resolution functions (see Results section hereinbelow). Under these conditions, the function result is considered an estimate of the degree of focus at the corresponding position. A fit,

20   or weighted average, of the data was performed during testing. Based on the ideal shape of the focus data, curve fits to a Gaussian and second and third order polynomials were tested. In each case, data were found with relatively aberrant shapes that caused the curve fits to perform very badly. The unusually shaped curves were probably produced by discrete distributions of cellular components in

25   the vertical direction, causing a series of local maxima. For these reasons a weighted average of the form

22

$$ W_a = \frac{\sum_z z F_z^n}{\sum_z F_z^n} \tag{1} $$

where w_a is the weight-averaged position, z is the vertical position (and to be
distinguished from a specific function as such notation is used elsewhere herein),
F is the result of a preselected autofocus function calculated from an image
acquired at one position, and n is the power of the weighing, is used. The power

5   accentuates the peak values. Over a narrow search range of 1 or 2 μm with
increments significantly smaller than the depth of field, the function values are
similar, and low powers result in best foci that are very close to the average z. To
improve sensitivity to the peak value, the power 'n' is increased to 4 and 8 before
reasonable sensitivity to the maximum is achieved. These steps are shown in the

10   flowchart of Figure 6 and are explained above.

Sequential autofocus has an advantage over binary autofocus. Each focus
position tested is defined before the focus routine begins. There is no dependence
on the focus function value at previous positions. Therefore, delays, such as
between integration of the image on the video camera 108 and digitization in the

15   image processor 110, do not slow execution of the focus routine as much as they
would with the binary search.

In sequential autofocus, the focus position is moved to a series of locations,
and at each location the image is acquired, filtered, and histogrammed. Based on
the histogram, a single focus value is calculated and stored. When the focus test

20   sequence is complete, a power-weighted average of the focus function values is
used to calculate best focus. Unlike binary autofocus, the calculated best focus
position may lie in-between the tested positions.

Both of autofocus methods assume that focus lies within a predetermined
range. Most of the time, this is true in scanning microscopy because each new

23

field is directly adjacent to the previous one. If best focus lies at or near the ends of the range, the probability that it actually lies outside the range is higher. In the sequential autofocus method, if the best focus does lie close to the ends, the range is moved and autofocus process is repeated.

5   II. <u>METRICS FOR PERFORMANCE: AUTOFOCUS FUNCTIONS</u>

Image content autofocus functions are based on the assumptions that images increase in contrast and resolution (edge sharpness) as focus improves. In the contrast model, with an image that consists of light and dark regions, the light regions become darker and the dark regions become lighter as the equipment is

10   moved farther from focus. This change in contrast can be described mathematically by the change in variance or standard deviation of pixel intensity. In the resolution model, detail blurs as the image moves out of focus. Resolution can be measured by analyzing the Fourier frequency spectrum or by the application of gradient, or highpass filters that isolate the high frequencies. The magnitude

15   of the high frequencies or gradients can then be used as a measure of resolution, which is defined as a maximum at best focus. The effects of the defocusing on the optical transfer function have been discussed by others, such as Born and Wolf (Born M, Wolf E: Principles of Optics, 6th Edition, Pergamon Press, New York, 1989), Erteza (Erteza A: Sharpness index and its application to focus control.

20   Appl Opt, 15:877-881, 1976; Erteza A: Depth of convergence of a sharpness index autofocus system. Appl Opt 16:2273-2278, 1977), Goodman (Goodman JW: Introduction to Fourier Optics. McGraw-Hill, New York, 1968), Groen et al., loc. cit., and Hopkins (Hopkins HH: The frequency response of a defocused optical system. Proc Roy Soc A 231:91-103, 1955). Vollath, loc. cit., 1987, and (Vollath

25   D: Verfahren und Einrichtung zur automatischen Scharfein-stellung eines jeden Punktes eines Bildes. German Patent DE 2,910,875 C 2, U.S. Patent 4,350,884,

24

1982, European Patent 0017726) derived additional autofocus functions based on autocorrelation and then suggested modifications for reducing the effects of noise.

The eleven autofocus functions that were tested are summarized in Table 1, along with references and calculation times on the computer hardware used here.

5   The functions are divided into the following groups: 1) measures of resolution (F_1 - F_4), which are the sum of the squares of the result of a highpass filter; 2) measures of contrast (F_5, F_6), represented by intensity variance or standard deviation, 3) combined measures of resolution and contrast (F_7, F_8), and 4) autocorrelation functions (F_9 - F_{11}), which also incorporate components of

10   resolution and/or contrast. The theory supporting the referenced functions is discussed by the respective authors. For mathematical description of these functions, the image is represented by g_{ij} where i and j are the spatial coordinates and g is the pixel intensity and all sums are double over i and j. In the equations, the dependence of the image and the autofocus function on vertical position is

15   assumed (i.e., a function value is calculated from the image at each position).

25

Table 1
Autofocus Functions

Function	Calculation Time[*] Frames/Position
1. Resolution	
$F_1 = \sum_{ij} ([1 \ 0 \ -1] * g_{i,j})^2$	1
$F_2 = \sum_{ij} ([1 \ -1] * g_{i,j})^2$	1
$F_3 = \sum_{ij} ([-1 \ 2 \ -1] * g_{i,j})^2$	1
$F_4 = \sum_{ij} \left(\begin{bmatrix} -1 & -2 & -1 \\ -2 & 12 & -2 \\ -1 & -2 & -1 \end{bmatrix} * g_{i,j} \right)^2$	1
2. Contrast	
$F_5 = \sigma^2 = \dfrac{1}{n(n-1)} (n \sum_{ij} g_{i,j}^2 - (\sum_{ij} g_{i,j})^2)$	1
$F_6 = \sigma$	1
3. Resolution and Contrast	
$F_7 = \dfrac{1}{n(n-1)} (n \sum_{ij} P_{i,j}^2 - (\sum_{ij} p_{i,j})^2)$	
where $P_{i,j} = \begin{bmatrix} -1 & -1 & -1 \\ -1 & 9 & -1 \\ -1 & -1 & -1 \end{bmatrix} * g_{i,j}$	1,5[††]
$F_8 = \sqrt{F_7}$	1,5[††]
4. Autocorrelation	
$F_9 = \sum_{ij} g_{i,j}^2 - \sum_{ij} g_{i,j} g_{i+1,j}$	4
$F_{10} = \sum_{ij} g_{i,j} g_{i+1,j} - \sum_{ij} g_{i,j} g_{i+2,j}$	8
$F_{11} = \dfrac{1}{n(n-1)} (n \sum_{ij} g_{i,j} g_{i+1,j} - (\sum_{ij} g_{i,j})^2)$	8

[*] Convolution operation.
$n = i \cdot j$, the total number of pixels in the image.
[†] RS-170 video format, '1' corresponds to calculation at the same rate as A/D conversion, 1 frame = 33 ms, 1 field = 16 ms.
[††] 1 frame time if convolution result is absolute value truncated to 8 bits, and 5 frame times if 16- bit signed.

26

All of these functions utilize the entire image, rather than only the cells. In fluorescence, the cells, or objects, could be roughly identified using a threshold, and focus calculated from only the object pixels. This would add complexity, however, and slow autofocus. Since positioning is 2 fields ahead of function

5   calculation, interposing the requirement to threshold the features and build a mask would cause a delay of at least a few frames. There could also be other problems. The distinct, bright nucleus becomes a dim, amorphous blur away from best focus. Even when this dim blur is barely discernible by eye, the direction to best focus can be easily determined by the algorithm used here. This is true well below the

10   intensity where thresholding would yield a reliable object. Also, the apparent object size increases out of focus, so thresholding at one position would not yield the same set of object pixels as thresholding at another. In phase contrast, segmentation of the cell features from image background would be much more difficult than a simple threshold, especially with the image out of focus. In

15   preliminary experiments, it was observed that even with no cells in the field, the presence of small amounts of cellular debris was enough to keep the system in focus. This is probably because the large number of pixels dramatically improves the signal-to-noise ratio. For these reasons, it is advantageous to utilize the entire image for focus calculation.

20   Independence from changes in illumination is desirable. For phase contrast, the result at each position was divided by the mean or the square of the mean intensity, matching the order of the function dependence on intensity, to compensate for lamp fluctuations. For fluorescence, such a scaling is ill-behaved because mean intensity nears 0 not far from focus and it is a better measure of

25   focus than of lamp intensity. Therefore, the functions were not similarly scaled for fluorescence autofocus. To correct for lamp fluctuations in fluorescence, independent measurement of lamp intensity are required.

27

The tested autofocus functions were chosen based on evaluations by other investigators and available computer hardware. Functions such as the thresholded absolute gradient and the thresholded video-signal content by Mendelsohn and Mayall (Mendelsohn ML, Mayall BH: Computer-oriented analysis of human

5   chromosomes-III focus. Comput Biol Med 2:137-150, 1972) were not tested because performance was shown by Groen et al., loc. cit., to depend in part on the arbitrary choice of a threshold. The entropy function, such as described by Shannon (Shannon CE: A mathematical theory of communications. Bell Sys Tech J 27:379-423, 623-656, 1948) was shown by Firestone et al. (Firestone L, Cook

10   K, Culp K, Talsania N, Preston K: Comparison of autofocus methods for automated microscopy. Cytometry 12:195-206, 1991) to be multimodal. Firestone et al., loc. cit., also tested the log spectral moment and two cellular logic functions that were not chosen because of hardware considerations. The log spectral moment requires the Fourier transform, which is still expensive to calculate at or

15   near real time, and the cellular logic functions require different hardware than was available here for fast implementation. Variations of highpass filtering have also been implemented in analog circuitry by others, such as Dew, King and Mighdoll (Dew B, King T, Mighdoll D: An automatic microscope system for differential leukocyte counting. J Histochem Cytochem 22:685-696, 1974) and Johnson and

20   Goforth (Johnson E, Goforth LJ: Metaphase spread detection and focus using closed circuit television. J Histochem Cytochem 22:536-545, 1974).

A. Functions Based on Resolution

Groen et al., loc. cit., reported F_1, F_2, and F_5 to be the best of 11 functions tested for brightfield microscopy. F_1, the squared gradient function

25   described by others, such as Brenner et al. (Brenner JF, Dew BS, Horton JB, King T, Neurath PW, Selles WD: An automated microscope for cytologic research. J Histochem Cytochem 24:100-111, 1976), Erteza, loc. cit., and Muller and

28

Buffington (Muller RA, Buffington A: Real-Time Correction of Atmospherically Degraded Telescope Images Through Image Sharpening. J Opt Soc Am 64:1200, 1974), is an implementation of the first derivative of the image intensity. In spectral terms, this is a bandpass filter that enhances frequencies just below the

5 highest in the image. Squaring the sum magnifies the differences between function values.

F_2 is the 1D Laplacian also described by Erteza, loc. cit., and Muller and Buffington, loc. cit. This filter is a measure of the second derivative of the image intensity. By operating on immediately adjacent pixels, F_2 has more predominant

10 highpass frequency characteristics than F_1, measuring resolution at a smaller scale. A variation of the Laplacian, based on lateral inhibition in the eye, was also evaluated by others, such as Harms and Aus (Harms H, Aus HM: Comparison of digital focus criteria for a TV microscope system. Cytometry 5:236-243, 1984). F_3 is the sum of the squares of the difference filter as described by Erteza, loc. cit.,

15 and Muller and Buffington, loc. cit. By operating on *both* immediately adjacent pixels, F_3 has the most predominant highpass frequency characteristics and measures resolution at the smallest scale. The use of similar derivative filters is explored by others, such as Shazeer and Harris (Shazeer D, Harris M: Digital Autofocus Using Scene Content, in Architectures and Algorithms for Digital Image

20 Processing II, SPIE 534:150-158, 1985). F_4, a common 2D Laplacian not previously tested, was added for comparison. With square pixels, F_4 would have been a mixture of the highest frequencies, corresponding to the horizontally and vertically adjacent pixels, and the next highest frequencies, corresponding to the diagonally adjacent pixels. With the rectangular pixels and larger vertical

25 sampling period of the RS-170 camera, however, this filter mixed in lower frequencies and did not have a higher frequency response than F_3.

B. Functions Based on Contrast

29

F_5, the statistical variance of the intensity as a measure of contrast, was proposed by, for example, the Kernforschungszentrum Karlsruhe GmbH (Kernforschungszentrum Karlsruhe GmbH: Verfahren und Einrichtung zur Automatischen Scharfeinstellung eines jeden Bildpunktes eines Bildes. Patent

5   Specification PLA 7907 Karlsruhe, 1979). F_6 is the standard deviation of the intensity, or the square root of F_5. It should be noted that under some conditions contrast achieves a local minimum, rather than a maximum, at best focus. The interference fringes that cause this are more commonly observed in transmission electron microscopy. With the light microscope, one way to observe this

10   phenomenon is by using phase contrast to image a micrometer (e.g., 0.85 NA 40x objective and 10 μm spacing). Best focus is at a local contrast minimum, and interference produces a series of contrast maxima and minima as focus is changed. Thus, contrast as a measure of focus must be utilized with caution in specimens with nonrandom spacing viewed in brightfield microscope modes.

15   C. Functions Based on Combined Resolution and Contrast

        F_7 and F_8 combine the variance and standard deviation, respectively, and a 3 x 3 sharpening filter. As pointed out by others, such as Vollath (Vollath D: The Influence of the Scene Parameters and of Noise on the Behavior of Automatic Focusing Algorithms. J Microsc 152(2):133-146, 1988), the frequency spectrum

20   is independent of the variance. That is, the variance can be changed by scaling the intensities without altering the relative Fourier power spectrum. The converse is not true: filtering the image can change the contrast. Thus, the image statistics measure a property fundamentally different from the Fourier spectrum, or sharpness of the image. This suggested using the variance (or standard deviation)

25   as the basic autofocus measure and modifying the frequency effect by prefiltering the image. The fact that hardware capable of calculating the variance of a filtered

30

image at video rates is becoming common makes consideration of this class of autofocus functions appropriate.

D. Functions Based on Autocorrelation

Correlation can be used to align images by multiplying them at different

5   relative shifts and summing the resulting pixels. A maximum occurs when the images are correctly aligned. Similarly for autofocus, if an image is multiplied by itself shifted D_i, D_j, a maximum in the correlation function occurs at $D_i = 0$, $D_j = 0$. Vollath, loc. cit., 1987 and 1982, pointed out that if the correlation function at $D_i = 0$, $D_j = 0$ is compared with the correlation function with the image shifted

10   with respect to itself, say $D_i = 1$, $D_j = 0$, the difference increases as image contrast increases. Therefore a maximum in the correlation function, F_8, should occur at best focus. Vollath, loc. cit., 1988, then made analogies between F_8 and the variance, F_3, to obtain F_9 and F_{10}. These correlation functions apparently have not been previously tested on biologic microscope images.

15   III. PERFORMANCE RESULTS

To determine the suitability of the various functions using the sequential autofocus process of Figure 6, each was first tested on selected microscope fields for both phase contrast and fluorescence microscopy. In preliminary experiments it was noted that the shapes of the focus function plots were dependent on the

20   number of cells in the field. In particular, it was found that a field containing a single small cell produced significantly different results than a field containing several cells. For this reason tests were performed on both types of fields. It was also found that the results were dependent on magnification, even using the same objective. Therefore, tests were performed at a series of magnifications by

25   changing the zoom on the relay lens. From these experiments on selected fields, functions were chosen for phase contrast and fluorescence autofocus, compared in

31

experiments scanning many fields and evaluated for accuracy, precision, reliability and speed.

A. Evaluation of Autofocus Functions on Selected Microscope Fields

1. Microscope Field with Ten Cells

5   The autofocus functions were first tested on a microscope field containing ten cells. The focus was changed in 0.098 μm increments (4 out of 4096 digital steps in a 100 μm range), and at each position the functions were evaluated for both phase contrast and fluorescence before moving to the next position. Figure 7 shows the plots of scaled function value versus position for fluorescence. While

10   there are clear variations in peak widths and sharpness, the functions are primarily unimodal. Only functions dependent on statistical measures (Figures 7e, 7f and 7i) show side peaks, and those are probably not significant enough to cause an algorithm to focus incorrectly. These small side peaks also appear in the mean intensity (Figure 7e). The repeating pattern of these peaks indicates that they are

15   probably due to interference, rather than lamp fluctuations.

       Table 2 summarizes the peak widths and best focus of each function for fluorescence. The widths at 90% of maximum show a clear dependence on the frequency characteristics of the function. Functions F_1, F_2 and F_3 are ordered from lowest to highest frequency enhancement and the peak widths narrow with higher

20   frequency, giving F_3 the narrowest peak. F_9, which looks similar to F_2 in spatial filter terms, also has very similar 50% and 90% widths. The resolution functions have very narrow peaks, whereas the contrast functions have much wider peaks. The combination functions, F_7 and F_8, offer a trade off, with narrower peaks than the contrast functions and wider ranges than the resolution functions. The

25   maxima, or best foci, for the predominantly statistical functions, F_5, F_6 and F_{11} differ by 1.07 μm from the others. Although one field is inadequate to determine

32

the significance of this difference, it raises the possibility that measures of contrast and resolution might not give the same focus.

Table 2

Autofocus Performance: Fluorescence, 10 Cells

Function	Widths (μm) at Percent of Peak		Ratio 50%/90%	Best Focus
	50%	90%		
F1	5.20	1.85	2.8	48.742
F2	4.95	1.70	2.9	48.742
F3	3.33	1.13	2.9	48.742
F4	4.95	1.65	3.0	48.742
F5	9.86	2.96	3.3	47.668
F6	16.20	4.20	3.8	47.668
F7	6.10	2.45	2.5	48.742
F8	11.00	3.35	3.3	48.742
F9	5.00	1.70	2.9	48.742
F10	5.28	2.00	2.6	48.742
F11	9.90	2.95	3.4	47.668

The phase contrast results from the same experiment on a field with ten cells are shown in Figure 8 and Table 3. In Figure 8 it is immediately obvious that the peaks are not as sharp and that the plots are more irregular. There is a tendency toward side peaks in all the plots and these are especially prominent in Figures 8e and 8i with the statistical functions. It can also be seen that the tendency toward side peaks is reduced by higher frequency response filters, with progressive reduction in the first shoulder from F_1 through F_2 and F_3 in Figures 8a, 8b, and 8c. The same trends as with fluorescence are visible in the peak widths.

33

That is, the highest frequency response filters, F_3 and F_4, also have the narrowest peaks and the contrast functions have very wide ranges.

Table 3

Autofocus Performance: Phase Contrast, 10 Cells

	Widths (μm) at Percent of Peak		Ratio	Best
Function	50%	90%	50%/90%	Focus
F1	5.73	1.95	2.9	49.621
F2	5.55	1.92	2.9	49.621
F3	5.35	1.88	2.8	49.621
F4	5.34	1.80	3.0	50.012
F5	22.05	2.55	8.6	49.915
F6	37.95	3.35	11.3	49.915
F7	5.54	1.90	2.9	50.012
F8	8.00	2.20	3.6	50.012
F9	5.55	1.95	2.8	49.621
F10	5.77	2.09	2.8	49.621
F11	26.25	3.20	8.2	49.915

2. Microscope Field with One Cell

The next experiment was performed in the same way on a microscope field containing a single cell. From the fluorescence data shown in Figure 9 and Table 4, it can be seen that the peaks are narrower. This is probably caused by the reduced distribution of cellular components in the vertical direction. With more cells, it is more likely that portions will extend farther from the coverslip. This may be even more true with a nuclear stain as used here, since the nucleus usually causes a spherically shaped cellular bulge and is not directly adherent to the glass as is the cell membrane. When the depth of field is comparable to cell thickness, the width of the focus function will certainly depend on specimen thickness. Furthermore, functions F_2 and F_3 show 90% peak widths of only 0.12 μm in Table 4. This is considerably less than the theoretical depth

34

of field of 0.74 μm. It may be because each result is a sum of a large number of pixels that is then squared. Summing a large number of pixels (245,760) increases the signal-to-noise ratio significantly. Squaring narrows the peaks further. The depth of field derivation by Born and Wolf, loc. cit., p. 441, assumes a 20% loss
5   in vertical resolution at the extremes of the focal section as measured by attenuation of the central image patch. Evidently the signal-to-noise characteristics of this implementation allow significantly better discrimination than a 20% change.

Table 4

Autofocus Performance: Fluorescence, Single Cell

10

Function	Widths (μm) at Percent of Peak 50%	90%	Ratio 50%/90%	Best Focus
F1	2.95	1.06	2.8	49.719
F2	2.10	0.12	17.5	49.817
F3	1.65	0.12	13.7	49.817
F4	4.28	1.01	4.2	49.719
F5	13.68	3.15	4.3	49.426
F6	17.85	5.10	3.5	49.426
F7	5.81	1.16	5.0	49.426
F8	12.78	1.76	7.3	49.426
F9	2.13	0.30	7.1	49.817
F10	3.45	0.40	8.6	49.719
F11	13.00	3.55	3.7	49.231

From Table 4, there were again differences between maxima, or best
25   foci, with the largest between the statistical functions and highpass filters. These differences, however, are less than with the data from the field with ten cells, raising the possibility that specimen thickness may have played a role.

The phase contrast data from the single cell experiment are shown in Figure 10 and Table 5. From Figure 10, it appears that phase contrast focus on
30   a field with a single cell offered the most severe autofocus challenge. All the plots exhibit significant side peaks and some appear quite noisy ("noisy" here is

35

descriptive only; it is probably *not* true that image noise caused this appearance). The statistical functions F_5, F_6 and F_{11} in Figures 10e and 10i are both noisy and have the largest side peaks. F_4 in Figure 10d also appears noisy. At first glance it was tempting to attribute the noisy appearance of F_4 to the frequency

5   characteristics of the highpass filter. However, as noted before, the frequency response of a camera with rectangular pixels lowers the vertical frequencies, complicating attempts to explain the cause. F_7 and F_8 in Figure 10f, mixtures of resolution and contrast functions, also appear noisy. The simple highpass filters F_1, F_2 and F_3 in Figures 10a, 10b, and 10c are smooth and exhibit the earlier

10   observed decrease in side peaks with increasingly high frequency response. From Table 5, there are again some differences in best foci, but these differences are small.

Table 5

Autofocus Performance: Phase Contrast, Single Cell

Function	Widths (μm) at Percent of Peak 50%	90%	Ratio 50%/90%	Best Focus
F1	4.85	1.42	3.4	51.282
F2	4.12	1.23	3.3	51.282
F3	3.40	1.03	3.3	51.282
F4[†]	——	——	——	51.477
F5	8.40	1.88	4.5	51.477
F6	8.62	2.00	4.3	51.477
F7[†]	——	——	——	51.477
F8[†]	——	——	——	51.477
F9	4.53	1.21	3.7	51.282
F10	5.30	0.62	8.5	51.282
F11	11.82	2.30	5.2	51.477

[†] Widths could not be determined due to multimodality (see Fig. 4)

36

Some indications of the sensitivity of the functions to lamp fluctuations in phase contrast can be seen in Figures 8 and 10. In both of the corresponding experiments, there were intensity spikes. In Figure 8e, there is a mean intensity spike at the position of about 87 μm, and in Figure 10e, one at near

5   55 μm and another at 85 μm. The mean intensity spike in Figure 8e showed up in F_4, F_7, and F_8 in Figures 8d and 8f and slightly in F_5, F_6 and F_{11} in Figures 8e and 8i. The resolution functions F_1 - F_3 in Figures 8a-8c and the autocorrelation functions F_9 and F_{10} in Figures 8g and 8h appear to have been immune from this lamp fluctuation. This same pattern is exhibited in Figure 10. It is interesting to

10   note that, with the exception of F_5, the functions that were sensitive to these lamp fluctuations are dependent on the contrast measures of variance or standard deviation.

        3. Function Dependence on Magnification and Sampling The data for phase contrast focus on a single cell suggested that the frequency response of

15   the focus function plays an important role in the formation of side peaks. It is likely that these side peaks arise from interference just above and just below best focus. Interference would be expected occur at lower frequencies since the departure from best focus degrades the modulation transfer function (MTF) of the microscope creating a lower frequency cut off. If a focus function measured only

20   the highest frequencies it should be immune from these effects. The focus function, however, is only one source of the frequency response. The microscope and the camera also have characteristic frequency responses that act prior to the focus function. Ideally, the camera should sample with at least twice the maximum frequency of the optical signal, according to the Nyquist sampling

25   criterion. The Rayleigh resolution estimate, has been explained by others, such as Inoué (Inoué S, Video Microscopy. Plenum Press, New York, 1986) is

37

$$d=\frac{1.22\lambda}{NA_{obj}+NA_{cond}} \qquad\qquad (2)$$

where λ is the wavelength of light and NA is the numerical aperture. With a 0.52 NA condenser, a 0.75 NA objective, and a peak wavelength of 540 nm corresponding to the peak transmittance of the daylight filter utilized, the resolution was 0.518 μm. Thus, the image should have been magnified so that the

5 distance between components of the specimen projected onto adjacent pixels corresponded to about 0.25 μm in the specimen. At a zoom of 1.0 with these optics, the projected distance was 0.607 μm. This represents a condition of undersampling and causes aliasing. Achieving Nyquist sampling would have required a zoom of 0.607/0.250 = 2.43, above the maximum available zoom of

10 2.25.

Unfortunately, the limited brightness in fluorescence microscopy can make Nyquist sampling highly impractical and even impossible. Intensity is proportional to the inverse square of the magnification and even with the bright preparation used here, a zoom of 2.25 forces operation of the camera and image

15 processor at the upper limits of gain, resulting in a very noisy signal. Limited fluorescence intensity motivates the use of high NA, low magnification objectives that increase the problem of undersampling. Because of the signal loss with increased magnification, it is impractical to optimally sample for autofocus in fluorescence and undersampling conditions were maintained for these experiments.

20 It is important, however, to understand the effects of sampling on autofocus, since many objectives and microscopes with different magnifications and NA's are available. To further study the dependence of the side peaks on magnification, an experiment on a microscope field with a single cell was carried out at a series of zooms, 0.9 - 2.25, that correspond to a range of 37 - 93%

25 undersampling. A 3D plot of the response of function F_3 versus focus position and

38

zoom is shown in Figure 11. At a zoom of 0.9 the side peaks are big enough to cause an autofocus algorithm to locate a spurious best focus under some conditions. As predicted, increasing the magnification to nearly optimal sampling at 2.25 caused the side peaks to disappear. This experiment underscores the fact
5   that the choice of optics and camera can be very important in determining focus function characteristics: anything that changes the resolution or the magnification will cause similar changes.

It was also observed, for example, that growing the cells on the coverslip instead of the slide increased the size of the side peaks (data not shown).
10   This was due to the gain in resolution from placing the cells at the location where objective aberrations are best corrected as described by others, such as Gibson (Gibson SFF, Modeling the 3-D Imaging Properties of the Fluorescence Light Microscope, Ph. D. Dissertation, Carnegie Mellon University, Pittsburgh, Pennsylvania, 1990). The index of refraction of the mounting media, thickness of
15   the coverslip, dirt in the optical path, illumination wavelength, and camera and image processor electronics are other components that can alter the system MTF, such as described by Inoué, and change the shape of the focus function.

B. Autofocus Performance in Automated Scanning

Finally, phase contrast and fluorescence autofocus were tested in a
20   series of experiments scanning rectangular areas of > 1000 fields. The purpose of these experiments was to test the hypothesis that the weighted average is a good estimate of best focus, measure autofocus precision, determine how small a number of focus positions could be used without compromising precision in an attempt to achieve maximum speed, and compare the best focus between phase contrast and
25   fluorescence.

Several rectangular areas on different specimens were scanned in a raster pattern, with refocusing performed 20 times in fluorescence and then 20

39

times in phase contrast. F_3 was used in phase contrast for all experiments and either F_3 or a variation of F_7, where the filter was [-1 2.5 -1], were used for fluorescence. These choices were based on consideration of peak sharpness and unimodality. With scanning microscopy, a operation over a large vertical range

5   is not as important because the best foci of adjacent fields are usually not far apart. In addition, those functions resulting in the largest range also had problems with unimodality on a single cell in phase contrast. Therefore, the highest frequency response filter was chosen for phase contrast. For fluorescence, F_3 gave a narrow enough range with a single cell (1.03 μm 50% peak width from Table 5) to be a

10   problem even for scanning microscopy. Therefore, F_7 and F_3 were considered good candidates. Since the real-time implementation utilized the interlaced camera signal, the variation of F_7 substituting a 1D sharpening filter for the 2D filter was used.

1. Accuracy, Precision and Speed

15   For each set of 20 autofocus tests, mean and standard deviation were calculated for both the maximum and the weighted average of best focus. The differences between the means of the maxima and weighted averages were also calculated to determine if the weighted average was a comparatively accurate estimate of best focus.

20   The results of these tests are shown in Figure 12. From the combined standard deviations, the autofocus precision in phase contrast averaged 0.154 μm with the maximum and 0.069 μm with the weighted average. In fluorescence the precision averaged 0.230 μm for the maximum and 0.159 μm for the weighted average. This is considerably better than the 0.74 μm depth of field

25   of the 20x, 0.75 NA objective. In all but the first experiment the precision was better with phase contrast than with fluorescence. There are a number of factors that could have contributed to this difference. In phase contrast, the image was

40

strobed near the end of the video field after the piezoelectric focus had stopped at its new position, whereas in fluorescence, each field was integrating on the CCD while focus was changing (30 - 50% of the field duration). Also, as previously discussed, the cellular and nuclear components may have been distributed
5   differently.

The statistics from the difference of the maxima and weighted averages showed a very good agreement between the two estimates of best focus. In phase contrast, the differences ranged from -0.025 to 0.014 μm and the largest standard deviation was 0.071 μm. In fluorescence, the differences ranged from -
10   0.002 to 0.044 with a maximum standard deviation of 0.088 μm. Given this agreement between the two estimates and the improvement in combined standard deviation, it is clear that the weighted average was a better measure of best focus.

The above performance was obtained with focus times as short as 0.25 second (s) in phase contrast. There appeared to be no degradation in focus
15   precision at 0.25 s with 11 focus positions tested. Therefore, even faster autofocus may be possible.

2. Phase Contrast Focus as an Estimate of Fluorescence Focus

The differences between the means of each set of focus tests in phase and fluorescence are shown in Table 6. Excluding experiment 2, where the
20   fluorescence autofocus lost track for part of the scan, the average of the differences between the two microscope modes varied between -0.394 and 0.745 μm, with good agreement between the maxima and weighted averages. There are many possible causes of this difference in foci, including microscope alignment, focus sampling interval and differences between nuclear and cytoplasmic component
25   distributions. These results indicate that measuring and correcting for the difference between the two microscope modes may yield significant improvement. It did not seem possible, however, to predict the difference from one specimen to

41

another. Again excluding experiment 2, the average standard deviation was 0.347 μm for the maximum and 0.342 for the weighted average. Thus the standard deviation of the difference was about 1/2 the depth of field of the objective. Although this might be enough to cause a small loss of precision in fluorescent 5 measurements, it indicates that phase contrast autofocus provided a good estimate of fluorescence autofocus.

Table 6

Comparison of Best Focus between
Phase and Fluorescence in Automated Scanning

10   Mean Phase - Mean Fluorescence

Maximum Weighted Averages

Experiment	Mean		Mean	
1	0.292	0.420	0.293	0.410
2*	0.934	1.150	0.985	1.140
3	0.719	0.235	0.745	0.219
4	-0.183	0.142	-0.196	0.137
5	-0.394	0.457	-0.349	0.465
6	-0.214	0.397	-0.175	0.400
7	-0.301	0.433	-0.304	0.423

All measurements in microns.
* Fluorescence autofocus lost track for a portion of the scan.

IV. CONCLUSIONS

The experiments carried out with the presently preferred embodiment of the 25 autofocus system of the present invention showed that it is possible to scan large areas of a microscope slide using phase contrast autofocus to minimize exposure for fluorescence imaging. This should make possible the imaging of living cells with minimal toxicity and the analysis of sensitive fluorescence preparations without photobleaching while focusing. There was a significant difference

42

between best focus in phase contrast and fluorescence, but the difference was constant enough to allow correction. In addition, it was shown that autofocus can be performed with precision an order of magnitude better than the depth of field in less than 0.25 s. Improved precision was achieved using the weighted average,

5   which made use of the data from all focus positions tested.

The power-weighted average is the average of the positions, each weighted by a power of the focus value at that position. The weighted average is calculated from the array of focus function results. Each focus function result is a magnitude resulting from calculation of the function over the entire image frame (245,760

10   pixels) or field (122,880 pixels) at a single position. The maximum does not account for the magnitude of the values at adjacent positions, while the weighted average does by averaging the function values at all positions.

This performance was achieved after minimizing the effects of undersampling by choosing autofocus functions with the most prominent highpass

15   filter characteristics. The problem of undersampling could be even more severe with lower magnification, high NA objectives and higher NA condensers. Multimodality was even more severe for functions less dependent on resolution and particularly severe with contrast measures. The lack of unimodality with intensity variance (or standard deviation) in phase contrast autofocus makes use of

20   contrast-based functions more questionable. The interference postulated to cause this problem may be present with all forms of transmitted microscopy where the image elements are small in number or regularly spaced.

For fluorescence, the fact that brightness is also directly dependent on distance from best focus may overwhelm the unwanted interference contrast

25   extrema. All autofocus functions tested here decrease in magnitude with decreasing image intensity. The attenuated fluorescence may decrease or eliminate multimodality in the contrast measures of focus. The highpass filter functions have an even narrower range because of this intensity dependence. By combining

43

the statistical and resolution measures, the range can be broadened while retaining a relatively narrow peak. Such a combination may be important for scanning sparsely populated cell specimens and necessary for autofocus applications requiring greater operating range.

5   The level of autofocus reliability and speed achieved here is an important step in bringing measurements common in flow cytometry closer to practical use in scanning cytometry. Such measurements may have advantages related to *in situ* analyses, such as morphology, relationship and position not possible with flow cytometry. Position may be a particular advantage for time lapse analysis of living

10   cells where cell-by-cell tracking would be possible with short scan intervals.

AUTOFOCUS USING VOLUME IMAGING WITH CONTINUOUS SCANNING

      The speed of my autofocus technique may be increased with a volume imaging apparatus that continuously acquires an image of the volume of an image object that is being examined by a microscope. The image includes a set of

15   images obtained at respective two-dimensional image planes that are offset vertically. Hereinafter such an image is referred to as a "volume image" or a "three-dimensional image".

      This embodiment is based upon my critical realization that a volume image of a portion of an image object being examined by microscope can be obtained by

20   an apparatus that includes (1) a plurality of imaging devices, each imaging device positioned at a respective image plane of a plurality of substantially parallel image planes, where each image plane is displaced in a particular dimension with respect to each other image plane, and (2) an image forming apparatus coupled to the plurality of imaging devices that forms a plurality of electronic image

25   representations, each electronic image representation representing an image at a respective image plane of the plurality of image planes.

44

Each electronic image representation represents a section of the image object that is displaced in the particular dimension from all other sections of the same image object.

To support autofocus in a scanning microscope, the volume imaging
5   apparatus is scanned continuously ahead of a specimen imaging apparatus. Both the volume imaging apparatus and the specimen imaging apparatus observe the same image object through the same microscope optics. Therefore, autofocus can be implemented by the analytical methods of my autofocus technique described above with respect to Figures 1-12. As will become clear, the volume imaging
10   apparatus does not require incremental positioning of the microscope in the Z dimension in order to obtain a volume image. Therefore, it is not necessary to stop at each microscope field to obtain a set of images by incrementally positioning the microscope stage in the Z dimension. Accordingly, this embodiment achieves a very important objective of speeding up my autofocusing
15   technique illustrated in Figures 1-12.

Figure 13 illustrates, in hybrid block/schematic form, the invention in a system that fully automates continuously-scanning autofocusing in a microscope 390. The microscope 390 comprises two overlapping optical systems, one for volume imaging, and one for fluorescence imaging. Preferably, the microscope
20   390 is an epifluorescent upright microscope (such as that described above with reference to Figure 1) with phase contrast optics. The fluorescence imaging optical system includes an epi-illumination light source 410 which illuminates an image object, with the aid of a collector lens 412 and a relay lens 414, a fluorescence filter block 415, with its emission interference filter removed and
25   placed at 448, and a piezoelectric-positioned objective lens 418 that is adjustable bidirectionally along the arrow 419. The epi-illumination provided by the light source causes an image object (in this case, a microscope field 420 with cells) to fluoresce, with the fluorescent emissions passing through the objective lens 419

45

and the filter block 415 to a dichroic mirror 430 which reflects the fluorescent emissions through the interference filter 448 and a relay lens 432 onto a CCD camera 433. The output of the camera 433 is provided to a cytometry processor 434 for processing fluorescent images of the cells in the microscope field 420.

5   The volume-imaging optical system includes a trans-illumination light source 400 that provides illumination of the image object for phase-contrast optics including a collector lens 402 and a relay lens 404, a mirror 406 which reflects the trans-illumination through a wide band pass interference filter 407 (for example, a 600 nm ± 50 nm bandpass filter) which separates light used for autofocusing

10   from the fluorescence excitation and emission wavelengths (typically, 365nm and 480nm for DAPI). Manifestly, the trans-illumination wavelength can easily be changed to accommodate other fluorescence wavelengths. The trans-illumination light is separated from the emitted fluorescence light by the dichroic mirror 430 and imaged through the relay lens 435 with a volume imaging apparatus that

15   includes a volume imaging array 436 and an array of cameras 437. The cameras of the array 437 can comprise, for example, time-delay-and-integration (TDI) CCD cameras. Preferably, the cameras of the array 437 operate in parallel, with their outputs (hereinafter, "electronic image representations") converted from analog to digital (A/D) format through A/D circuits 440. The parallel converted electronic

20   image representations are provided from the A/D circuit 440 to a volume image processor 442 (that includes storage 443) for calculating a best focus from the electronic image representations of the camera array 437. The best focus output of the volume image processor 442 is provided to a piezoelectric objective positioner controller 446 that operates a piezoelectric objective positioner 447.

25   The piezoelectric objective positioner 447 positions (or repositions) the objective lens 418 at (to) the current best focus position as determined by the volume image processor 442.

46

The microscope 390 is motorized by means not shown for scanning in the xy plane and for movement on the Z axis as indicated by the axes 439. In this respect, the microscope 390 is identical with the microscope 102 of Figure 1.

The optical principle of volume imaging according to the invention may be
5   understood with reference to Figure 14A and Figure 14B. Volume imaging is based on the idea that within a reasonable vertical distance (several microns) of best focus at an image forming microscope plane ("image object plane") is an in-focus volume consisting of adjacent optical planes. This can be demonstrated by a simple experiment performed on a microscope with a video camera and display.
10   First, an image object is placed in focus and displayed on the display. Then the video camera is moved a short distance along the optical axis. This will cause the image to defocus. Next, with the new position of the video camera retained, the focus knob on the microscope is adjusted to reacquire sharp focus. This image object-objective focal distance is changed by a few microns in this last step. Thus,
15   relative to the objective face, a new optical plane is brought into focus. Within a reasonable vertical distance, this does not degrade optical performance. The means for parallel acquisition of such an image volume is shown in Figures 14A and 14B.

In Figure 14A, there is shown an array 470 of optical light pipes (optical
20   fibers). The optical light pipes of the array 470 are coupled to an array 474 of CCD cameras. In this regard, each optical light pipe has two ends, a first end being held together with corresponding first ends of the other optical light pipes in a stepped array that is magnified in Figure 14B, and a second end connected to a respective CCD camera. For example, the optical light pipe 472 includes first
25   and second ends, 473 and 474, with the second end 474 coupled to the CCD camera 475. The optical light pipe 476 includes first and second ends 477 and 478, with the second end 478 connected to the CCD camera 479. The first ends 473 and 477 of the optical light pipes 472 and 476 are held together in the stepped

47

array illustrated in Figure 14B. As Figure 14B shows, the first ends of the optical light pipes, including the ends 473 and 477 are disposed in substantially longitudinal array, with each respective first end being positioned at a respective image plane of a plurality of image planes. For example, the end 473 is

5   positioned at an image plane designated as Z_1, while the end 477 is positioned at a second image plane denoted as Z_2. Figure 14B shows that, for n light pipes, the stepped, substantially longitudinal array of optical light pipe first ends defines a corresponding array of image planes where each image plane is displaced in a particular direction (the Z dimension of this embodiment) with respect to each

10   other image plane. Thus, the image plane Z_1 is vertically upwardly displaced from the image plane Z_2, while the image plane Z_n is vertically downwardly displaced from the image planes Z_1 and Z_2. The stepped array of first ends is offset in the Z direction from an image object plane (a surface of a microscope slide, for example) on which an image object (a stained cell, for example) rests.

15   Manifestly, each optical light pipe constitutes an imaging device and each camera is an image forming apparatus. Referring again to Figure 13, the array of optical light pipes 470 corresponds to the volume imaging array 436 of Figure 13, while the array 474 of CCD cameras corresponds to the camera array 437 of Figure 13.

20   Figures 15A and 15B illustrate a second embodiment of a plurality of imaging devices according to the invention in the form of a linear image sensor 481 having a linear array 482 of active photo elements, such as the photo element 485. The image sensor 480 is tilted with respect to an image object plane 488 where an image object is located so that each photo element intersects a respective

25   image plane which is displaced in the vertical dimension with respect to each other image plane. Thus, in Figure 5B, the image plane Z_i is intersected by a photo electric element 485, while the image plane Z_{i+1}, offset by vertical distance d, is intersected by another photo electric element 486. With this embodiment of

48

imaging devices, the images are formed by CCD camera electronics which operate
in the same manner as the electronics of the cameras in the array 474 of Figure 13.

With reference now to Figure 13, Figure 14A and Figure 14B, the
microscope 370 includes a conventional stage upon which a microscope slide 438

5   is carried. The microscope slide 438 is prepared for fluorescent cytometry as
described above and is scanned over a plurality of microscope fields in a raster
pattern automatically as described above. Such scanning is in the xy plane of the
axes 439. With the stage moving at a constant velocity in x, adjacent image
planes are sampled by the cameras of the CCD camera array 474 with small,

10   successive time delays. These delays are removed by buffering. The fluorescence
image acquired for analysis is collected with a longer delay as shown in Figure 5
to allow for the piezoelectric repositioning time, for example, a maximum of 10
msec, or < 100 micrometer travel in a 500 micrometer square field with a 20x
objective. Focus can be calibrated by measuring the difference between the

15   fluorescence image acquired for analysis and the volume image acquired for
focusing. In this regard, the differences between the best fluorescence and volume
imaging focuses may be measured by repeated scans at slightly different focus
levels to compute focus directly from the fluorescence images. The fluorescence
focus position may then be set to eliminate the difference between the best focus

20   in fluorescence and volume imaging for subsequent scans.

As shown in Figure 16, the stepped ends of the optical light pipe array 470
form a volume imager field of view (FOV) that scans in the scan direction over
a portion of a microscope field such as the field 490. Trailing behind the volume
imager FOV is a fluorescent imager FOV. With respect to the volume imager

25   FOV, consider a slice of the field having an aspect ratio approximately
corresponding to that of each of the rectangular first ends in the stepped array of
optical light pipe ends including the ends 473 and 477. The slice is indicated by
Δ_i in Figure 16. As the image planes Z_1-Z_n are scanned over the slice, a two-

49

dimensional image of the slice is captured by each optical light pipe/CCD camera combination. The image can comprise one or more pixels. Each image, denoted as P, is stored (as an electronic image representation) in a buffer corresponding to the slice in the manner shown in Figure 17. Thus, for a set of successive buffer

5   locations in the buffer for the slice Δ_i ("the Δ_i buffer"), as each first end face of the stepped end face array shown in Figure 14B is scanned over the slice, an electronic image representation representing a two-dimensional image at the image plane of an end face is stored at a storage location corresponding to the end face. Thus, an image P_1 formed at image plane Z_1 corresponding to the end face 473 of

10   the optical light pipe 472 is stored in the Δ_i buffer at the position corresponding to image plane Z_1. In this manner, as the stepped end faces of the optical light pipe array 470 are scanned over the slice, a plurality of electronic image representations P_j are stored in the Δ_i buffer. As Figure 17 shows, there are buffers provided for an array of slices. Figure 18 shows a volume image stored

15   in the Δ_i buffer formed by electronic image representations of the two-dimensional images P_1-P_n obtained through the image planes Z_1-Z_n, respectively.

It may be appreciated that an advantage is gained when the volume image is acquired by "tilting" at the image plane (by offsetting the image planes in the vertical direction) rather than by directly tilting the microscope slide. The

20   advantage is due to the fact that vertical magnification is the square of lateral magnification. In the embodiment illustrated in Figures 1-12, for example, magnification to the video camera CCD chip is about 30x. Therefore, the vertical magnification is about 900x and a 4 μm thick volume of a specimen would be magnified to 3.6 mm at the image plane. This exaggerated vertical magnification

25   simplifies precise sampling of the required optical sections.

I have calculated dimensions of the step array of optical light pipe ends illustrated in Figure 14B based upon assumptions about the dimensions of image objects and available CCD camera technology. The dimensions of this array

50

(shown in Figure 14B) were calculated assuming a 4 μm thick specimen volume magnified through a 20x objective and a 0.9x-2.25x zoom relay lens (available from Nikon) onto 1024 pixel x 96 line TDI CCD arrays with 13 x 13 μm pixels. However, design considerations, particular requirements of an application, and changes in optical and camera technology will manifestly vary these assumptions. Nevertheless, assuming relatively rigid optical light pipes, a well-supported, single package that integrates the optical light pipes with the CCD cameras is required for the embodiment illustrated in Figure 14A and 14B. The package is not shown, but may consist, for example, of a rectangular aluminum frame attaching to both the CCD cameras and the optical light pipes. Assuming a relatively small remote CCD camera (such as a 2.0" x 2.0" x 0.75" camera available from Dalsa) these components may be placed in a conveniently sized package.

The dimensions shown in Figure 14B include a vertical step of 0.017" between optical light pipe end faces for convenience in assembly. This corresponds to a 29.387x lateral magnification and an 863.6x vertical magnification. Using the zoom lens described above, this magnification corresponds to a zoom of 1.04x (out of a possible range of 0.9x-2.25x). A 20x phase/fluorite objective having a field of view with a 710 μm diameter for a 502 μm inscribed square field may be used. Such a field therefore would be magnified to 14.75 mm (0.58") square at the proposed lateral magnification. This leaves ample room for a trailing CCD that acquires the fluorescence image. The CCD cameras are disclosed as being of the TDI type to increase light sensitivity, which permits the dwell time to be reduced for continuous scanning.

Manifestly, there will be light loss through the optical light pipe interfaces. However, this can be compensated adequately by the brightness range of conventional transmitted microscope lamps. Use of TDI cameras may also decrease a small percentage of random rearrangements of optical fibers common in optical light pipe interfaces and problems with Moire patterns that can occur

51

with improper matching of such optical fibers and at the camera arrays. As is known, any Moire set will be averaged out by TDI cameras. The 2:1 binning of the TDI cameras, both for fluorescence and phase contrast, may also eliminate undersampling and aliasing, without the loss of light accompanied by the usual

5   method of limiting the effective numerical aperture (NA).

Figure 19 illustrates the processing that is used to determine an optical quality metric by processing the image representations according to an autofocus function described in the incorporated patent application. Preferably, the function is a resolution function (described in Table 1) which sums the squares of the result

10   of highpass filter (HPF). Relatedly, the squared values of the electronic image representations provide augmented intensity values. As Figure 19 shows, an electronic image representation representing an image at a respective image plane is acquired at the output of a CCD camera at step 501, digitized at step 503, and buffered at step 504. The sequence 501, 503, 504 continues until an electronic

15   image representation for each image plane of a plurality of image planes is acquired and buffered. A measure of resolution is acquired by summing the squares of the result of highpass filtration of the digitized images in steps 505 and 506. A focus metric is constructed in step 507 and the image plane where the best focus occurs as indicated by the focus metric is chosen in step 508 and the

20   microscope is refocused by the autofocus mechanism, if necessary. A representative focus metric is illustrated in Figure 20 as a plot of a sharpness index indicating the measure of resolution at each image plane.

Calculation of the optical quality metric (resolution, or sharpness) requires processing of the image representations. Assuming nine image planes such as

25   would be acquired by the stepped end face of Figure 14B, nine parallel electronic image representations would have to be processed. In combination, this would produce a 90 MHz pixel rate that must be processed in parallel. Preferably, for each electronic image representation, a 1 x 3 convolution (- 1 2 - 1) will be

52

applied for high pass filtration, followed by calculation of the sum of the squares. Manifestly, the volume image processor (442 of Figure 13) should be capable of processing the image representations in parallel. Such parallel processing is well-supported by pipeline image processors such as the Imaging Technology MVC 40

5   MHz image processor. Such a system comprises a set of mother boards, each having a three-channel, eight-bit A/D converter, image buffers, and processing pipelines. For example, nine image streams can be processed in an Imaging Technology processor by three sets of mother boards.

The volume image processing of the invention can be further improved by

10   relocating the highpass filtration function. For example, in the embodiment of the autofocus system illustrated in Figure 21, the highpass filtration function is located in the optics of the microscope 390 at a backfocal, Fourier or pupil plane. In this embodiment, the plurality of imaging devices comprise an array 610 of photo elements that corresponds to the tilted linear array of high sensitivity photo electric

15   elements shown in Figure 15A and Figure 15B. In this case, the array 610 of photo electric elements is coupled to camera electronics 620. In the embodiment of the autofocus system illustrated in Figure 21 (in which reference numerals identical with those in Figure 13 represent identical elements), the volume image processor 442 processes highpass filtered electronic image representations to

20   produce the optical quality metric; this processor is simplified in that the electronic image representation output by the camera electronics 620 has the form of the integral $I_{x(t)z}$ shown in Figure 21. Manifestly, this integral reduces the cost of performing autofocus calculations, when compared with the volume imaging embodiment illustrated in Figure 13. In Figure 13, the volume image processor 442

25   must process many two dimensional image representations that make up the three dimensional image. With a highpass function is performed optically as shown in Figure 21, the electronic image representation processing is reduced. With the use of Fourier relay optics 602 to produce a projected pupil plane (which is a Fourier

53

transform plane), an optical highpass filter 605 can be implemented as an attenuation (amplitude), or phase filter. See "Optical Information Processing," (S.H. Lee, Springer-Verlag: New York, 1981) for the principles of optical filtration. In operation, the optical highpass filter 605 blocks the low frequency portion of an image. The high frequency, or edge information is retained, and the intensity of the high frequency information is proportional to focus. Thus, the intensity at a particular image plane provides a direct measure of sharpness and the focus metric of Figure 20 can be derived by simply plotting intensity (as sharpness) versus image plane. The intensity (sharpness) at many different image planes is measured using the tilted high sensitivity photo electric element array 610. This requires only a single image processor to buffer and remove delays from the electronic image representations and to calculate best focus. Essentially, the autofocus system embodiment of Figure 21 reduces the cost of implementation by replacing three image processing boards, nine CCD cameras and one optical light pipe array with one image processing board, one tilted photo electric element array, and one set of camera electronics.

Continuous volume imaging could also rapidly scan a volume using the confocal microscope principle, as with either slit or spot confocal apertures. With a slit aperture, longitudinal CCD arrays on the CCD cameras which form images at image planes may be illuminated through a slit confocal aperture. Assuming linear CCD arrays in each camera of a single pixel in width, each linear CCD array would image a single plane. However, the image object would be illuminated with a corresponding confocal slit of light for each linear CCD array, resulting in higher resolution, especially in the vertical direction, but also laterally. Thus, an array of stationary slits, each illuminating a respective image plane, in combination with moving a microscope stage at a constant velocity in one direction, will create a real-time volume-imaging confocal microscope. As with the array of confocal slits, an array of confocal spots such as is taught in U.S.

54

Patent 5,239,178 could also be arranged at different image plane positions and combined with stage scanning to create even higher resolution.

Clearly, other embodiments and modifications of the present invention will occur readily to those of ordinary skill in the art in view of these teachings. Therefore, this invention is to be limited only by the following claims, which include all such embodiments and modifications.

55

CLAIMS

1.   A method of autofocus for a microscope having a focus mechanism, the method comprising the steps of:

(1) acquiring a digital image of a specimen on a microscope stage at a first vertical position;

(2) applying a digital filter to the digital image to obtain a filtered image;

(3) applying a measurement function to the filtered image to obtain a magnitude;

(4) moving the focus mechanism in the vertical direction to a second vertical position and repeating steps (1)-(3); and

(5) comparing the magnitudes of the filtered images acquired at the first and second vertical positions so as to adjust focus of the microscope based on the comparison.

2.   The method defined in Claim 1, wherein the digital filter performs an image sharpening transformation.

3.   The method defined in Claim 1, wherein the measurement function measures contrast.

4.   The method defined in Claim 1, wherein the measurement function includes the step of calculating the sum of the filtered image intensities.

5.   The method defined in Claim 1, wherein the measurement function includes the step of calculating a sum of the squared filtered image intensities.

56

6. The method defined in Claim 1, wherein the comparing step includes the step of moving the focus mechanism toward the first vertical position if the magnitude at the first position is greater than the magnitude at the second position, and moving the focus mechanism toward the second vertical position if

5 the magnitude at the first position is less than the magnitude at the second position, thereby adjusting the focus of the microscope.

7. An apparatus for generating a volume image, comprising:

a plurality of imaging devices, in which at least one imaging device is positioned at a respective image plane of a plurality of image planes,

10 where each image plane is displaced in a third dimension with respect to each other image plane; and

an image forming apparatus coupled to the plurality of imaging devices for forming a plurality of electronic image representations representing images at respective image planes of the plurality of image

15 planes.

8. The apparatus of Claim 7, further including processing means coupled to the image forming apparatus for determining an optical quality metric by combining electronic image representations.

9. The apparatus of Claim 7, wherein the plurality of imaging devices

20 includes a plurality of optical conductors, each optical conductor having a first end face positioned at a respective image plane and a second end face coupled to the image forming apparatus.

10. The apparatus of claim 7, wherein the plurality of imaging devices are disposed in a substantially elongate array.

57

11.   The apparatus of Claim 7, wherein the image forming apparatus includes a plurality of charge-coupled device (CCD) cameras.

12.   The apparatus of Claim 11, wherein the plurality of imaging devices includes a plurality of optical conductors, each optical conductor having a first end

5   face positioned at a respective image plane of the plurality of image planes and a second end face coupled to a respective CCD camera.

13.   The apparatus of Claim 12, wherein each first end face is offset in the third dimension from each other second end face.

14.   The apparatus of Claim 7, wherein the plurality of imaging devices

10   includes an elongate array of photo electric devices.

15.   The apparatus of Claim 14, wherein the elongate array of photo electric devices is tilted with respect to an image object plane, each image plane of the plurality of image planes being intersected by at least one photo electric device of the elongate array of photo electric devices. .

15   16.   The apparatus of Claim 8, wherein the processing means includes:
            a plurality of image buffers, each image buffer for storing a plurality of electronic representations of at least a portion of an image;
            a high-pass filter coupled to a respective buffer for providing a filtered electronic representation; and
20   means coupled to the high-pass filter for combining a plurality of filtered electronic representations to produce the optical quality metric.

58

17.   The apparatus of Claim 16, wherein the means for combining includes:

means for obtaining augmented intensity values for the filtered electronic representations; and

5   means for indicating a value of the optical quality metric for each image based upon the augmented intensity values.

18.   The apparatus of claim 7, further including:

an optical high pass filter positioned between the plurality of imaging devices and an image object plane; and

10   processing means coupled to the image forming apparatus for determining an optical quality metric by combining electronic range image representations.

19.   The apparatus of claim 18, wherein the processing means includes:

a plurality of image buffers, each image buffer for storing

15   a plurality of filtered electronic image representations of at least a portion of an image; and

means coupled to the plurality of image buffers for combining a plurality of filtered electronic image representations to produce the optical quality metric.

20   20.   The apparatus of claim 19, wherein the optical quality metric is image sharpness.

21.   A method for volume imaging using a plurality of imaging devices in which at least one imaging device is positioned at an image plane of a plurality

59

of image planes, where each image plane is displaced in a third dimension with respect to each other image plane, the method comprising the steps of:

orienting the plurality of imaging devices such that the imaging devices observe an image object in an image object plane;

5   using the plurality of imaging devices, obtaining a plurality of images of the image object, each image of the plurality of images obtained in a respective imaging device;

converting the plurality of images into a plurality of electronic image representations; and

10   storing the plurality of electronic image representations.

22.   The method of Claim 21, wherein the plurality of imaging devices includes a plurality of optical conductors, each optical conductor having a first end face positioned at a respective image plane, the step of orienting including positioning the first end faces with respect to the image object plane such that each

15   image plane is substantially parallel to and vertically displaced from the image object plane.

23.   The method of Claim 21, wherein the plurality of imaging devices includes a plurality of photo electric devices disposed in an elongate array having a longitudinal dimension, the step of orienting including disposing the elongate

20   array of photo electric devices such that an extension of the longitudinal dimension intersects the image object plane at a non-orthogonal angle.

24.   An autofocus apparatus for autofocusing a microscope having a focus mechanism, the apparatus comprising:

a plurality of the imaging devices, at least one imaging device of

25   the plurality of imaging devices positioned at each respective image plane

60

of a plurality of image planes, where each image plane is displaced in a third dimension with respect to each other image plane;

an image forming apparatus coupled to the plurality of imaging devices to form a plurality of electronic image representations, each electronic image representation representing an image at a respective two-dimensional image plane of the plurality of image planes;

a processor coupled to the image forming apparatus for generating a focus location signal by applying a measurement function to the electronic image representations; and

means for causing the focus mechanism to adjust the focus of the microscope in response to the focus location signal.

25.   The autofocus of Claim 24, wherein the plurality of imaging devices includes a plurality of optical conductors, each optical conductor having a first end face positioned at a respective image plane and a second end face coupled to the image forming apparatus.

26.   The autofocus apparatus of Claim 24, wherein the image forming apparatus includes a plurality of charge-coupled device (CCD) cameras.

27.   The autofocus apparatus of Claim 26, wherein the plurality of imaging devices includes a plurality of optical conductors, each optical conductor having a first end face positioned at a respective image plane of the plurality of image planes and a second end face coupled to a respective CCD camera.

28.   The autofocus apparatus of Claim 24, wherein the plurality of imaging devices includes an elongate array of photo electric devices.

61

29.   The autofocus of Claim 28, wherein the elongate array of photo electric devices is tilted with respect to an image object plane at which an image object located, each image plane of the plurality of image planes being intersected by at least one photo electric device of the elongate array of photo electric devices.

5   30.   The autofocus apparatus of Claim 24, wherein the processor includes:

a plurality of image buffers, each image buffer for storing a plurality of electronic representations of at least a portion of the image each electronic representation representing an image of the portion at a
10   respective image plane of the plurality of image planes;

highpass filter means coupled to an image buffer for providing a plurality of filtered electronic image representations; and

means coupled to the high-pass filter means for combining a plurality of filtered electronic image representations to produce a focus
15   metric.

31.   The autofocus apparatus of Claim 21, further including an optical filter positioned between the plurality of imaging devices and an image object plane.

32.   The autofocus apparatus of Claim 31, wherein the processing means
20   includes:

a plurality of image buffers, each image buffer for storing a plurality of filtered electronic image representations of at least a portion of an image; and

62

means coupled to the plurality of image buffers for combining a plurality of filtered electronic image representations to produce the optical quality metric.

33.   The apparatus of claim 32, wherein the optical quality metric is
5   image sharpness.

34.   The autofocus apparatus of Claim 30, wherein the means for combining includes:

means for obtaining augmented intensity values for the filtered electronic image representations; and
10   means for indicating a value of the focus metric for each image based upon the augmented intensity values.

35.   A method for autofocus for a microscope having a focus mechanism, the method comprising the steps of:

acquiring a plurality of electronic image representations of an image
15   object on an image object plane, wherein each electronic image representation represents an image of the image object at a respective image plane of a plurality of image planes in which each image plane is displaced in a third dimension with respect to every other image plane;

applying the plurality of electronic image representations to a
20   highpass filter to obtain a plurality of filtered electronic image representations;

applying a measurement function to the plurality if filtered electronic image representations to obtain a plurality of image sharpness values;

63

combining the image sharpness values by relating the image sharpness values to image plane positions;

selecting an image plane position related in the combining step to a high image sharpness value; and

5   adjusting focus of the microscope based on the selected image plane position.

FIG. 1

FIG. 2

2/23

FIG. 3

3/23

START — 202

MOVE FOCUS MECHANISM
IN VERTICAL DIRECTION
TO NEW VERTICAL POSITION — 212

200

ACQUIRE DIGITAL IMAGE OF SPECIMEN
AT VERTICAL POSITION — 204

APPLY FILTER TO ACQUIRED IMAGE
TO PRODUCE FILTERED IMAGE — 206

APPLY MEASUREMENT FUNCTION TO
FILTERED IMAGE TO OBTAIN MAGNITUDE — 208

210 — Nth IMAGE ACQUIRED ?   NO

YES

COMPARE ACQUIRED MAGNITUDES AND ADJUST
FOCUS BASED ON COMPARISON RESULTS — 214

END — 216

FIG. 4

4/23

START — 252

250 ⟍

IF NOT AT CENTER, MOVE TO CENTER. ACQUIRE IMAGE
Fc=FOCUS FUNCTION RESULT
— 254

MOVE STAGE TO CENTER − RANGE/2. ACQUIRE IMAGE
Fa=FOCUS FUNCTION RESULT
— 256

MOVE STAGE TO CENTER + RANGE/2. ACQUIRE IMAGE
Fb=FOCUS FUNCTION RESULT
— 258

260 ⟍
IS
RANGE
< MINIMUM
?
— YES

NO

END — 272

FIG. 5

RANGE=RANGE/2 — 262

264 ⟍
IS
Fa>Fb
?

YES

NO → Fb IS ≥ Fa — 268

CENTER = CENTER − RANGE/2
MOVE STAGE TO CENTER
Fb=Fc
Fc=FOCUS FUNCTION RESULT
— 266

CENTER = CENTER + RANGE/2
MOVE STAGE TO CENTER
Fa=Fc
Fc=FOCUS FUNCTION RESULT
— 270

START —302

300

304 — START POSITION =
CENTER — RANGE/2   N = 0

306 — MOVE TO START POSITION + N(STEP SIZE)
ACQUIRE IMAGE
Fn = FOCUS FUNCTION RESULT

308 — IS
CURRENT
POSITION—START
POSITION ≤
RANGE
?

YES   n = n + 1

310

NO

COMPUTE BEST FOCUS FROM Fo ... Fn —312

314 — DOES
RESULT LIE
TOO CLOSE TO THE
BEGINNING OR END
OF THE RANGE
?

YES

316 — CHANGE CENTER
TO END OF RANGE
NEAREST TO
CALCULATED FOCUS

NO

318 — MOVE TO BEST FOCUS

320 — END

FIG. 6

$$F_1 = \sum_{ij} ([1 \quad 0 \quad -1]*g_{i,j})^2$$

FIG. 7A

$$F_2 = \sum_{ij} ([1 \quad -1]*g_{i,j})^2$$

FIG. 7B

$$F_3 = \sum_{ij} ([-1 \quad 2 \quad -1]*g_{i,j})^2$$

FIG. 7C

7/23

$$F_4 = (g_{i,j} * \begin{bmatrix} -1 & -2 & -1 \\ -2 & 12 & -2 \\ -1 & -2 & -1 \end{bmatrix})^2$$

FIG. 7D

$F_6 = \sigma$

IMAGE MEAN

$F_5 = \sigma^2$

FIG. 7E

$$F_7 = \sigma^2 \text{ OF } \begin{bmatrix} -1 & -1 & -1 \\ -1 & 9 & -1 \\ -1 & -1 & -1 \end{bmatrix} * g_{i,j}$$

$F_8 = \sqrt{F_7}$

FIG. 7F

$$F_9 = \sum_{ij} g^2_{i,j} - \sum_{ij} g_{i,j} g_{i+i,j}$$

FIG. 7G

$$F_{10} = \sum_{ij} g_{i,j} g_{i+i,j} - \sum_{ij} g_{i,j} g_{i+2j}$$

FIG. 7H

$$F_{11} = \frac{1}{n-1} \left\{ \sum_{ij} g_{i,j} g_{i+i,j} - \frac{1}{n} \left(\sum_{ij} g_{i,j} \right)^2 \right\}$$

FIG. 7I

9/23

FIG. 8A

$$F_1 = \sum_{ij}([1 \quad 0 \quad -1] * g_{i,j})^2$$

FUNCTION VALUE [0,1]

Z-POSITION (μm)

FIG. 8B

$$F_2 = \sum_{ij}([1 \quad -1] * g_{i,j})^2$$

FUNCTION VALUE [0,1]

Z-POSITION (m)

FIG. 8C

$$F_3 = \sum_{ij}([-1 \quad 2 \quad -1] * g_{i,j})^2$$

FUNCTION VALUE [0,1]

Z-POSITION (μm)

$FIG.$ $8D$

$$F_4=\left(g_{i,j} * \begin{bmatrix} -1 & -2 & -1 \\ -2 & 12 & -2 \\ -1 & -2 & -1 \end{bmatrix}\right)^2$$

FUNCTION VALUE [0,1]

Z-POSITION (μm)

$FIG.$ $8E$

IMAGE MEAN
(SCALED TO 1)

$F_6 = \sigma$

$F_5 = \sigma^2$

FUNCTION VALUE [0,1]

Z-POSITION (μm)

$FIG.$ $8F$

$$F_8 = \sigma^2 \text{ OF} \begin{bmatrix} -1 & -1 & -1 \\ -1 & 9 & -1 \\ -1 & -1 & -1 \end{bmatrix} * g_{i,j}$$

$F_7 = F_8{}^2$

FUNCTION VALUE [0,1]

Z-POSITION (μm)

FIG. 8G

$$F_9 = \sum_{ij} g^2_{i,j} - \sum_{ij} g_{i,j}\, g_{i+i,j}$$

FIG. 8H

$$F_{10} = \sum_{ij} g_{i,j}\, g_{i+i,j} - \sum_{ij} g_{i,j}\, g_{i+2j}$$

FIG. 8I

$$F_{11} = \frac{1}{n-1}\left\{ \sum_{ij} g_{i,j}\, g_{i+i,j} - \frac{1}{n}\left(\sum_{ij} g_{i,j}\right)^2 \right\}$$

$$F_1 = \sum_{ij} ([1 \ \ 0 \ \ -1] * g_{i,j})^2$$

FIG. 9A

$$F_2 = \sum_{ij} ([1 \ \ -1] * g_{i,j})^2$$

FIG. 9B

$$F_3 = \sum_{ij} ([-1 \ \ 2 \ \ -1] * g_{i,j})^2$$

FIG. 9C

FIG. 9D

$F_4 = (g_{i,j} * \begin{bmatrix} -1 & -2 & -1 \\ -2 & 12 & -2 \\ -1 & -2 & -1 \end{bmatrix})^2$

FUNCTION VALUE [0,1]

Z-POSITION (μm)

FIG. 9E

IMAGE MEAN

$F_6 = \sigma$

$F_5 = \sigma^2$

FUNCTION VALUE [0,1]

Z-POSITION (μm)

FIG. 9F

$F_7 = \sigma^2$ OF $\begin{bmatrix} -1 & -1 & -1 \\ -1 & 9 & -1 \\ -1 & -1 & -1 \end{bmatrix} * g_{i,j}$

$F_8 = \sqrt{F_7}$

FUNCTION VALUE [0,1]

Z-POSITION (μm)

14/23

FIG. 9G

$$F_9 = \sum_{ij} g^2_{i,j} - \sum_{ij} g_{i,j} g_{i+i,j}$$

FUNCTION VALUE [0,1]

1.0

0.5

0.0

0   25   50   75   100
Z-POSITION (μm)

FIG. 9H

$$F_{10} = \sum_{ij} g_{i,j} g_{i+i,j} - \sum_{ij} g_{i,j} g_{i+2j}$$

FUNCTION VALUE [0,1]

1.0

0.5

0.0

0   25   50   75   100
Z-POSITION (μm)

FIG. 9I

$$F_{11} = \frac{1}{n-1} \left\{ \sum_{ij} g_{i,j} g_{i+i,j} - \frac{1}{n} \left(\sum_{ij} g_{i,j} \right)^2 \right\}$$

FUNCTION VALUE [0,1]

1.0

0.5

0.0

0   25   50   75   100
Z-POSITION (μm)

FIG. 10A

$$F_1 = \sum_{ij}([1\ \ 0\ \ -1]*g_{i,j})^2$$

FIG. 10B

$$F_2 = \sum_{ij}([1\ \ -1]*g_{i,j})^2$$

FIG. 10C

$$F_3 = \sum_{ij}([-1\ \ 2\ \ -1]*g_{i,j})^2$$

FIG. 10D

$$F_4 = \left(g_{i,j} * \begin{bmatrix} -1 & -2 & -1 \\ -2 & 12 & -2 \\ -1 & -2 & -1 \end{bmatrix} \right)^2$$

FIG. 10E

IMAGE MEAN
(SCALED TO 1)

$F_6 = \sigma$

$F_5 = \sigma^2$

FIG. 10F

$F_8 = \sqrt{F_7}$

$$F_7 = \sigma^2 \text{ OF } \begin{bmatrix} -1 & -1 & -1 \\ -1 & 9 & -1 \\ -1 & -1 & -1 \end{bmatrix} * g_{i,j}$$

$$F_9 = \sum_{ij} g^2_{i,j} - \sum_{ij} g_{i,j} g_{i+i,j}$$

FIG. 10G

$$F_{10} = \sum_{ij} g_{i,j} g_{i+i,j} - \sum_{ij} g_{i,j} g_{i+2j}$$

FIG. 10H

$$F_{11} = \frac{1}{n-1} \{ \sum_{ij} g_{i,j} g_{i+i,j} - \frac{1}{n} (\sum_{ij} g_{i,j})^2 \}$$

FIG. 10I

FIG. 11

F_3

FOCUS
POSITION

PERCENT
NYQUIST

37%

93%

501 — CAMERA

503 — A/D

504 — BUFFER

WHILE
SCANNING Δ_i

HPF — 505

506
SUM OF SQUARES

507
FOCUS METRIC

508
CHOOSE BEST FOCUS
PLANE AND REFOCUS

FIG. 19

SHARPNESS INDEX

Z

FIG. 20

EXPERIMENTAL PARAMETERS

EXP'T	CELL DENSITY	FIELDS	FOCUS RANGE	FOCUS INCREMENTS	TIME (S)	PHASE/FLUOR FUNCTION
1	10%	1023	2.44	0.102	0.48	F_3/F_3
2	20%	1239	3.52	0.195	0.38	F_3/F_3
3	30%	1581	3.52	0.195	0.38	F_3/F_3
4	50%	1581	2.93	0.244	0.28	F_3/F_3
5	50%	1581	2.93	0.244	0.28	F_3/F_3
6	60%	1581	2.93	0.146	0.28	F_3/F_7
7	60%	1901	2.20(P)$#$ / 1.76(F)	0.220(P) / 0.073(F)	0.25(P) / 0.48(F)	F_3/F_7

$ P=PHASE;   F=FLUORESCENCE

PHASE CONTRAST

COMBINED σ		MAX-WA	
MAX	WA	MEAN	σ
0.210	0.097	0.002	0.059
0.160	0.071	-0.006	0.069
0.195	0.106	-0.007	0.045
0.093	0.041	0.014	0.027
0.139	0.061	-0.003	0.040
0.134	0.049	-0.025	0.057
0.148	0.059	0.002	0.071

FLUORESCENCE

COMBINED σ		MAX-WA	
MAX	WA	MEAN	σ
0.160	0.057	0.003	0.041
0.345	0.307	0.044	0.088
0.202	0.066	0.020	0.045
0.101	0.093	0.001	0.011
0.314	0.236	0.042	0.060
0.288	0.202	0.025	0.069
0.198	0.152	-0.002	0.036

FIG. 12
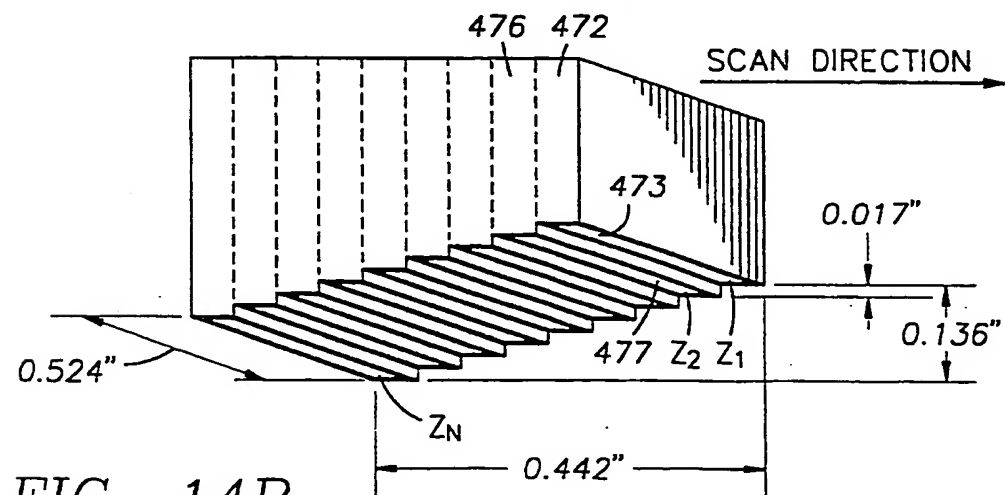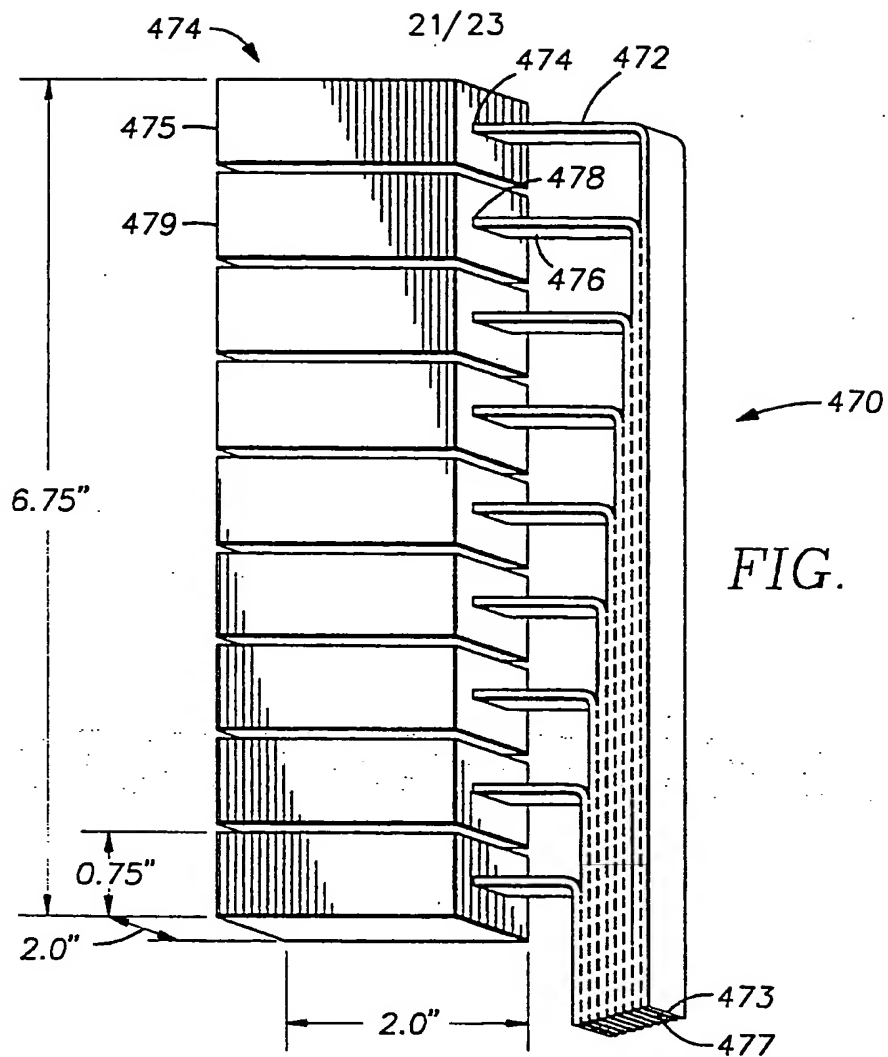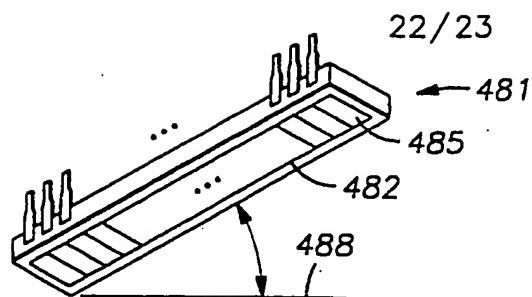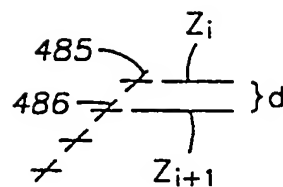
FIG. 13

21/23

FIG. 14A

FIG. 14B
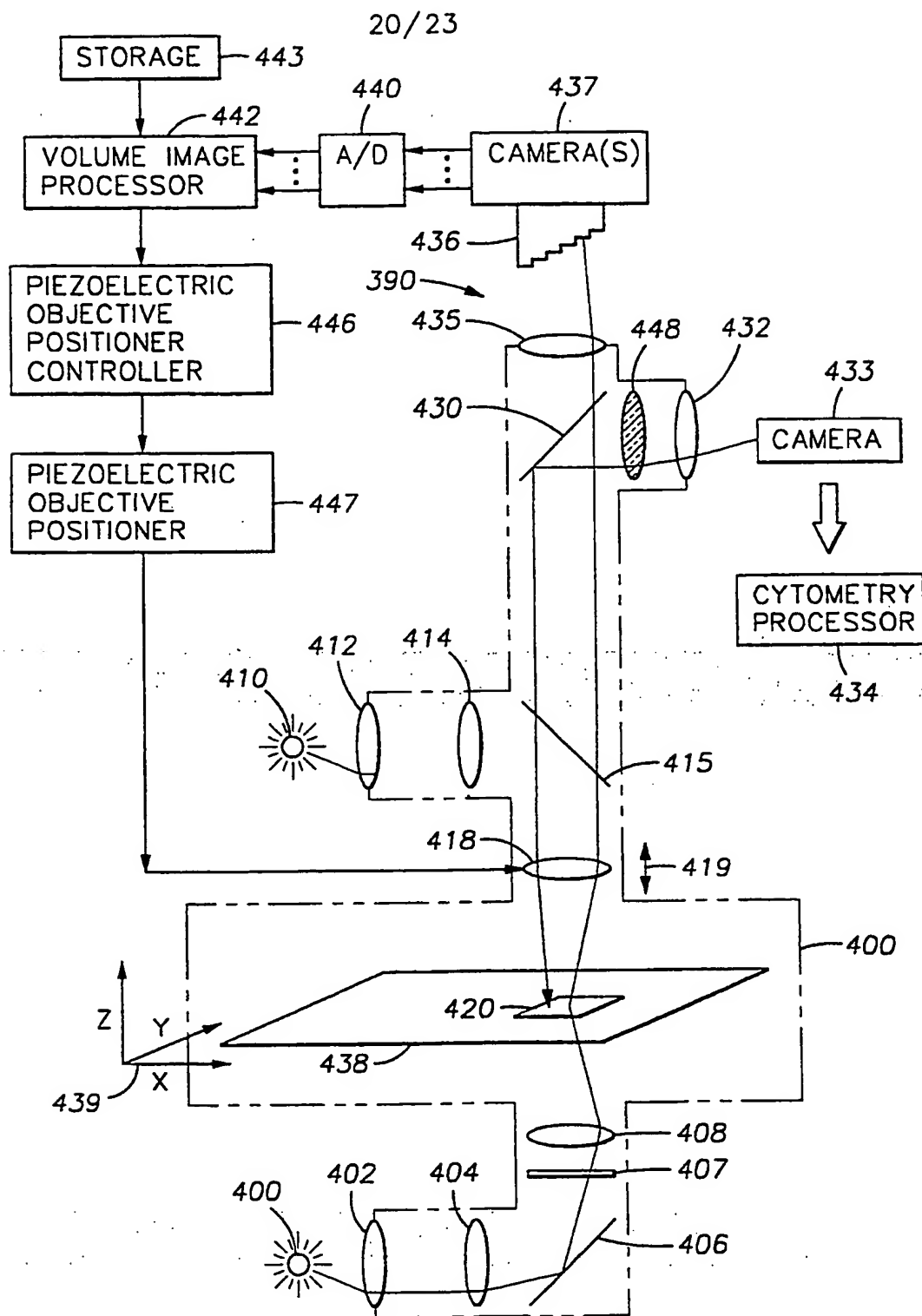
22/23

FIG. 15A

FIG. 15B

FIG. 16
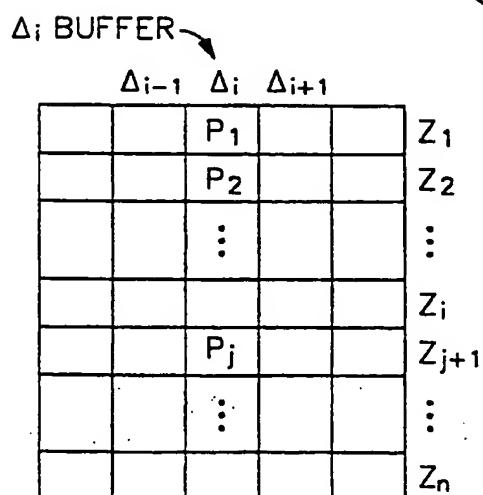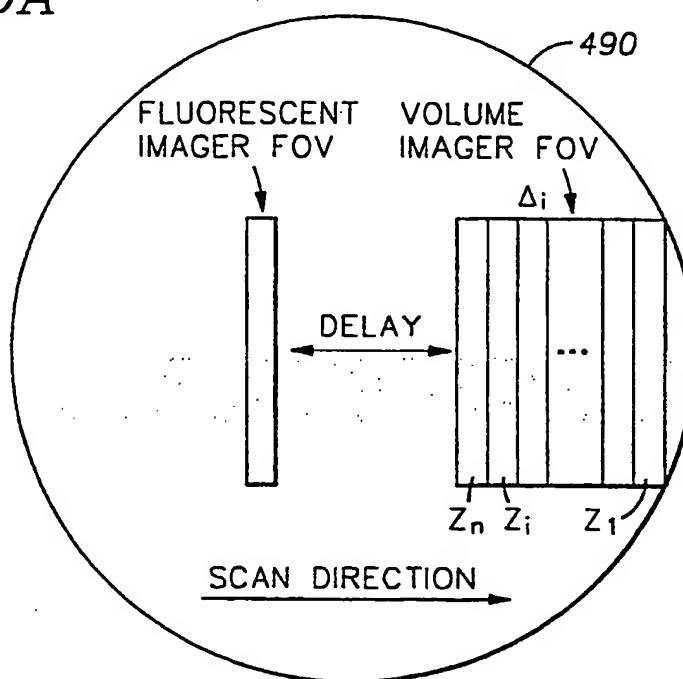
FIG. 17

FIG. 18

23/23
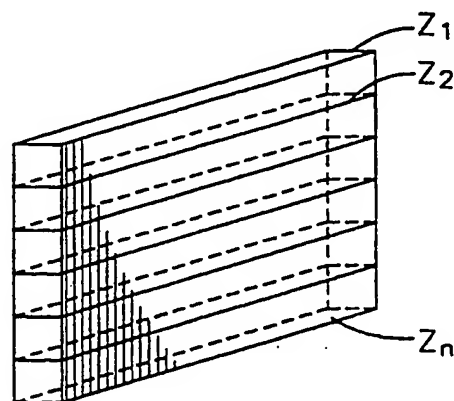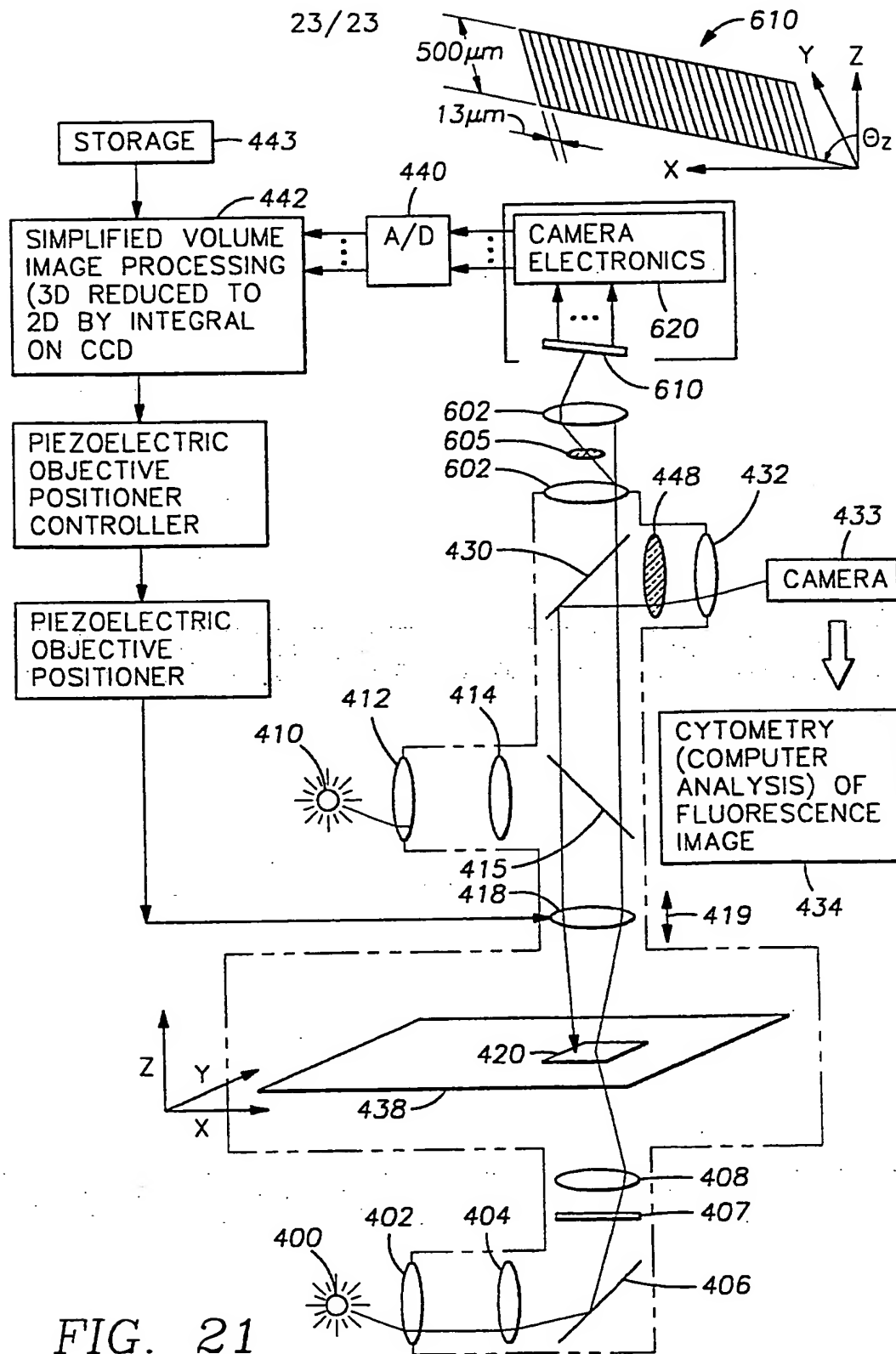
FIG. 21

	ational Application No
	PCT/US 95/08424

A. CLASSIFICATION OF SUBJECT MATTER
IPC 6   G02B21/24   G02B21/26   G02B7/36

According to International Patent Classification (IPC) or to both national classification and IPC

B. FIELDS SEARCHED

Minimum documentation searched (classification system followed by classification symbols)
IPC 6   G02B

Documentation searched other than minimum documentation to the extent that such documents are included in the fields searched

Electronic data base consulted during the international search (name of data base and, where practical, search terms used)

C. DOCUMENTS CONSIDERED TO BE RELEVANT

Category *	Citation of document, with indication, where appropriate, of the relevant passages	Relevant to claim No.
X	EP,A,0 163 394 (SHANDON SOUTHERN PRODUCTS) 4 December 1985	7,8,10, 11,14, 15,21, 23,24, 26,28,29
A	see the whole document	16-20, 30,34,35

X	DE,A,42 26 523 (BLOSS) 17 February 1994	7,8,10, 14,21, 24,28
A	see the whole document	1,16-20, 26,30,34

X	US,A,4 342 905 (FUJI ET AL) 3 August 1982	35
A	see the whole document	1,4,5,7, 21,24

	-/--	

X	Further documents are listed in the continuation of box C.	X	Patent family members are listed in annex.

* Special categories of cited documents :

"A" document defining the general state of the art which is not considered to be of particular relevance

"E" earlier document but published on or after the international filing date

"L" document which may throw doubts on priority claim(s) or which is cited to establish the publication date of another citation or other special reason (as specified)

"O" document referring to an oral disclosure, use, exhibition or other means

"P" document published prior to the international filing date but later than the priority date claimed

"T" later document published after the international filing date or priority date and not in conflict with the application but cited to understand the principle or theory underlying the invention

"X" document of particular relevance; the claimed invention cannot be considered novel or cannot be considered to involve an inventive step when the document is taken alone

"Y" document of particular relevance; the claimed invention cannot be considered to involve an inventive step when the document is combined with one or more other such documents, such combination being obvious to a person skilled in the art.

"&" document member of the same patent family .

Date of the actual completion of the international search	Date of mailing of the international search report
20 October 1995	27.12.95

Name and mailing address of the ISA	Authorized officer
European Patent Office, P.B. 5818 Patentlaan 2 NL - 2280 HV Rijswijk Tel. (+ 31-70) 340-2040, Tx. 31 651 epo nl, Fax (+ 31-70) 340-3016	Ward, S

Form PCT/ISA/210 (second sheet) (July 1992)

page 1 of 2

C.(Continuation) DOCUMENTS CONSIDERED TO BE RELEVANT

Category*	Citation of document, with indication, where appropriate, of the relevant passages	Relevant to claim No.
X	US,A,4 829 374 (MIYAMOTO ET AL) 9 May 1989	35
A	see the whole document	1,7,21, 24

X	DE,A,38 28 381 (CARL ZEISS) 15 March 1990	35
A	see the whole document	1,3,7, 21,24

X	DE,A,26 15 841 (CARL ZEISS) 13 October 1977	35
A	see the whole document	1,3,7, 21,24

A	US,A,5 239 170 (HUGHLETT) 24 August 1993 see the whole document	1
	-----	

ational Application No

PCT/US 95/08424

Patent document cited in search report	Publication date	Patent family member(s)		Publication date
EP-A-0163394	04-12-85	DE-A- JP-A- US-A-	3584314 60238805 4636051	14-11-91 27-11-85 13-01-87
DE-A-4226523	17-02-94	NONE		
US-A-4342905	03-08-82	JP-A- JP-B- JP-A- JP-A-	56035111 62032761 57037309 56062217	07-04-81 16-07-87 01-03-82 28-05-81
US-A-4829374	09-05-89	JP-A- DE-A-	63127148 3739027	31-05-88 19-05-88
DE-A-3828381	15-03-90	JP-A- US-A-	2118609 4958920	02-05-90 25-09-90
DE-A-2615841	13-10-77	AT-B- CH-A- GB-A-	351293 614292 1545437	10-07-79 15-11-79 10-05-79
US-A-5239170	24-08-93	NONE		

THIS PAGE BLANK (USPTO)